ISET JOURNAL of EARTHQUAKE TECHNOLOGY

Vol. 49 No. 1-2 March-June 2012

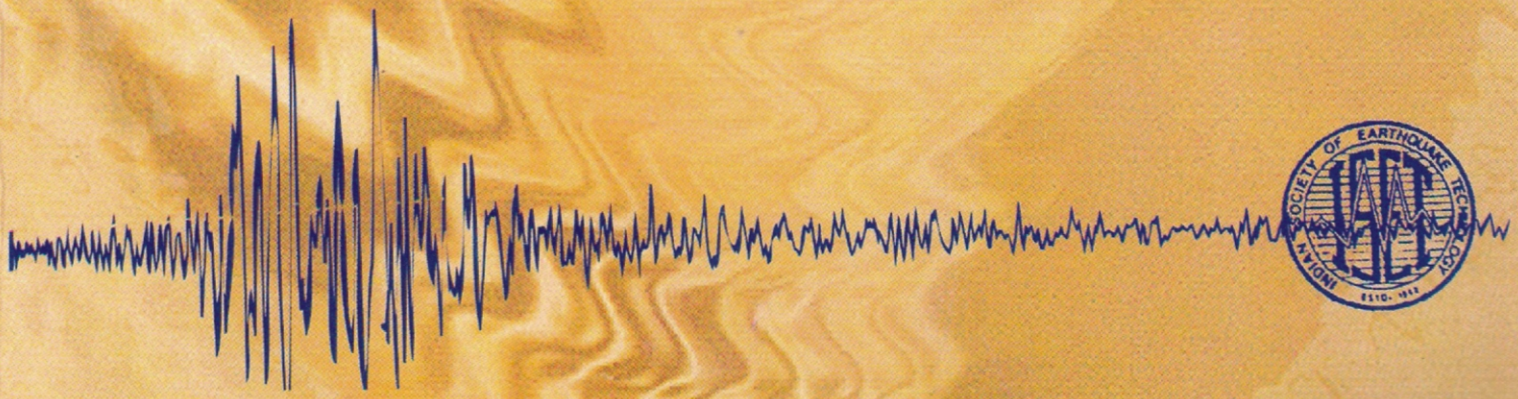

INDIAN SOCIETY OF EARTHQUAKE TECHNOLOGY
AIMS AND OBJECTIVES

i. To provide necessary forum for scientists and engineers of various specializations to come together and exchange ideas on the problems of earthquake technology.
ii. To disseminate knowledge in the field of earthquake technology dealing with seismological and engineering aspects.
iii. To promote research and development work in the field of earthquake technology.

ISET JOURNAL OF EARTHQUAKE TECHNOLOGY

The ISET Journal of Earthquake Technology is published quarterly in the months of March, June, September & December by the Indian Society of Earthquake Technology (ISET). It was first published in 1964 under the name of Bulletin of the Indian Society of Earthquake Technology and is renamed as ISET Journal of Earthquake Technology from the year 1998.

MEMBERSHIP AND SUBSCRIPTION

The membership of the Society is open to all Individuals and Institutions connected with or interested in any scientific, engineering and other aspects of Earthquake Technology.

For ISET members, subscription to the ISET Journal is included in the membership fee. The subscriptions are by annual volume only. The subscription rate for non-members is Rs.2000/- (US$ 200) per volume. Individuals and institutions may apply for membership on prescribed form obtainable from the Secretary on request. Back numbers of the previous Bulletins and the Journals, as in stock, can be obtained from the Secretary on full subscription payment. The rates per issue are given below:

For Non-Members	Rs. 750/- (US$ 50 by air mail)
For Special Issue	Rs. 1500/- (US$ 80 by air mail)

COMMUNICATION

Communications regarding change of address, subscription renewals, missed numbers, membership and Society publications should be addressed to the Secretary, Indian Society of Earthquake Technology, Department of Earthquake Engineering Building, IIT Roorkee, Roorkee-247 667, Uttarakhand, India, E-mail: ***office@iset.org.in; iset@iitr.ernet.in***

COPYRIGHT

MANUSCRIPT

Manuscript offered for publication in the ISET Journal should be submitted to the Editor. Members may also send news items, memoirs, book reviews and news about the activities of the ISET Local Chapters to the Co-Editor for publication in the ISET News Letter. Authors are given 25 reprints free of charge. Request for additional reprints, if desired, must be made immediately after acceptance of the paper is communicated to the authors. Reprints are supplied at the rate of Rs. 25/- (US$ 3) per reprint with a minimum charge of Rs. 500/- (US$ 75). The Society is not responsible for statements and opinions expressed by the authors in the Journal.

ISSN 0972-0405

ISET JOURNAL OF EARTHQUAKE TECHNOLOGY

Vol. 49 No. 1-2 March-June 2012

CONTENTS

No.	Paper	Page
518	Seismic Retrofit of Beams in Buildings for Flexure Using Concrete Jacket **V.T. Badari Narayanan, Amlan Kumar Sengupta and S.R. Satish Kumar**	1
519	NN-Based Damage Detection in Multi-storey Buildings from Modal Parameter Changes **Hemant Kumar Vinayak, Ashok Kumar, Pankaj Agarwal and Shashi Kant Thakkar**	23
520	Effect of Seismic Oblique Waves on Dynamic Response of an Embedded Foundation **Salah Messioud, Badreddine Sbartai and Daniel Dias**	37

Financial Assistance from DST, New Delhi for the Publication of ISET Journals for 2011–2012 and 2012–2013 is duly acknowledged

ISET Journal of Earthquake Technology, Paper No. 518, Vol. 49, No. 1-2, March-June 2012, pp. 1–22

SEISMIC RETROFIT OF BEAMS IN BUILDINGS FOR FLEXURE USING CONCRETE JACKET

V.T. Badari Narayanan, Amlan Kumar Sengupta and S.R. Satish Kumar

Department of Civil Engineering
Indian Institute of Technology Madras
Chennai-600036

ABSTRACT

To prevent disaster in future earthquakes, one way of retrofitting the members in reinforced concrete buildings is concrete jacketing. The present study investigates the effect of jacketing on the flexural strength and performance of beams. First, slant shear tests are conducted to study the interface between old and new concrete. Second, beam specimens are tested to study the effect of jacketing on the positive bending of the span region. Third, beam-column-joint sub-assemblage specimens are tested to study the effect of jacketing on the positive bending of the beams adjacent to the joint. Further, analytical investigations are carried out to predict the experimental results. A layered approach is used for the prediction of the moment versus rotation curves for the retrofitted beam specimens. An incremental nonlinear analysis is adopted to predict the lateral load versus displacement behaviour for the retrofitted sub-assemblage specimens. Finally, guidelines are provided for the retrofitting of beams by concrete jacketing.

KEYWORDS: Beam-Column-Joint Sub-assemblage, Beam, Concrete Jacketing, Layered Analysis, Retrofit, Seismic Force

INTRODUCTION

Recent earthquakes have exposed the vulnerability of reinforced concrete (RC) buildings. The earthquake at Bhuj, Gujarat in 2001 has been a watershed event in the earthquake engineering practice in India. The Indian code of practice for seismic analysis has been revised to reflect the increased seismic demand in many parts of the country. Many existing buildings lack the seismic strength and detailing requirements of the current codes of practice, because they were built prior to the implementation of these codes or due to limited technical expertise. Most recently, such deficiencies were observed in Sikkim after the earthquake at the Indo-Nepal border on 18th September, 2011.

The deficiencies in the buildings, which collapsed or were damaged during the Bhuj earthquake, were reported by Murty et al. (2002). A few other observations were made at the essential facilities in the Andaman Islands after the earthquake in 2004. The common deficiencies specific to beams in RC buildings include the following:

- Inadequate positive bending moment capacity adjacent to the beam-to-column joints. The longitudinal reinforcing bars (or rebars) at the bottom of a beam tend to be discontinuous or spliced at an interior joint. For an exterior joint, the bottom bars may not be bent properly with adequate hook length. The pull-out of the bars (especially under low axial load in the column) leads to a reduced capacity and deformability of the beam (see Figure 1).
- Inadequate amount and spacing of stirrups in the potential plastic hinge regions, leading to reduced shear capacity and ductility. The stirrups may not be designed to resist the shear corresponding to the development of the beam flexural capacity. The stirrups are generally open, unless the beam is designed for torsion. The stirrups may also be warped (i.e., not in a plane after bending the bar manually) and may lack adequate end hooks. These factors lead to an absence of confinement of the core concrete, especially in the absence of a slab on the side under compression.
- Short beams in narrow bays and transfer cantilevers (provided to support the floating columns above, which do not continue to the foundation) tend to fail in shear during an earthquake.
- Lower concrete strength than the design strength and concrete of poor quality with inadequate compaction lead to weakness in the plastic-hinge regions.

To prevent any disaster during the future earthquakes, the existing deficient buildings need to be retrofitted. The selection of an appropriate retrofit scheme is based on the seismic evaluation of a building and the available resources. For a building, a combination of retrofit strategies may be selected under a retrofit scheme.

Fig. 1 Failure in a beam due to pull-out of bottom reinforcing bars (at New Passenger Terminal, Port Blair, Andaman Islands, after the earthquake in 2004)

Various retrofit strategies may be broadly classified as local and global strategies. The global retrofit strategies are applied to improve the overall behaviour of the building. In addition to a global retrofit strategy, it may be necessary to also retrofit some members locally. One way of retrofitting the beams is by concrete jacketing. This involves placing an additional layer of concrete around the existing beam, together with additional longitudinal bars and stirrups, to enhance the flexural and/or shear capacities. The present paper reports an investigation into the strengthening of beams with bottom bars discontinuous at the joints. The objective of the study is to enhance the positive (or sagging) flexural capacity of the beams at the face of the joints by introducing additional continuous bottom bars. This study has been undertaken along with the investigation by Kaliyaperumal and Sengupta (2009) on strengthening of columns.

The other options of retrofitting a beam are the fibre-reinforced polymer (FRP) wrapping and the use of steel brackets or haunches. The application of FRP wraps is convenient and the increase in the size of the beam is minimal. The positive flexural capacity of a beam at the face of the joint can be increased based on the generated confinement of concrete and the pattern and strength of the wraps. However, the increase in capacity as well as the corresponding ductility can be limited. The deficiency due to the discontinuity of the bottom bars cannot be totally rectified. On the other hand, the use of steel brackets or haunches aims to shift the potential plastic hinge region in a beam away from the face of the joint. Although these schemes are effective, the use of exposed steel may be restricted based on the corrosion, fire and architectural considerations. In the present study, concrete jacketing is investigated as a viable option of introducing continuity of the bottom bars in a beam through the joint. This investigation is aimed to improve the positive flexural capacity of the beam at the face of the joint, along with retaining substantial ductility.

For an effective concrete jacket, the use of closed stirrups as dowels involves closely spaced drilling of the existing beam. If the latter is of low strength or poor quality or small width, the drilling may damage the member. Also, drilling may intercept the existing bars unless executed carefully with a rebar locator, such as a profometer. Hence, to minimize drilling, the use of closed stirrups is precluded and only preparation of the surface of the existing concrete is investigated in the present study on retrofit for flexure.

First, slant shear tests are carried out to check the interface bond between the existing (or old) and new concrete. From these results, it is found that the specimens with roughened surface of the existing concrete and without any bonding agent fail at higher loads compared to the other specimens. Thus, it is decided that for the retrofitted specimens, the faces of the existing concrete will be roughened by using a motorised wire brush and that bonding agent will not be used.

Second, simply supported flanged beam specimens are tested under the two-point monotonic and slow cyclic loadings to study the constructability and effectiveness of the selected jacketing scheme to enhance the positive flexural capacity in the span. However, the testing of such beam specimens does not

demonstrate their behaviour in frames near the joints under the seismic loads, which are dynamic and reversed cyclic in nature. The degradation of strength and stiffness of the beams, the deterioration of bond between the rebar and concrete especially near the joints, and the subsequent pull-out of the bottom bars cannot be simulated in the beam tests. Hence, beam–column−joint sub-assemblages are tested to study the effect of jacketing of the beams under positive bending near the joints.

In the conventional mechanics of reinforced concrete, a beam is analysed or designed by using the working stress method or the limit state method (including the strength method). However, for analysing and designing for seismic forces, a performance based approach is preferred. In the latter approach, not only the strength of a structural component is evaluated, but also the load versus deformation behaviour is quantified. Hence, in the present study an analysis method suitable for heterogenous sections is adopted to predict the behaviour of jacketed sections under a monotonic loading.

LITERATURE REVIEW

The general advantages of concrete jacketing in the context of construction in India are as follows (Chakrabarti et al., 2008):

- Jacketing by concrete can increase both flexural and shear capacities of a beam.
- The compatibility of deformation between the existing and new concrete, resistance against delamination, and durability are better as compared to a new material on a different substrate.
- Availability of personnel skilled in concrete construction.
- The analysis of retrofitted sections follows the principles of analysis of RC sections.

Of course, there are certain disadvantages of concrete jacketing, depending on the structure and its use:

- Increase in the size and weight of the beam.
- Anchoring of bars involves drilling of holes in the existing members.
- Manufacturing of sufficiently workable concrete for the jacket.
- Possibility of disruption to the users of the building.

Despite these disadvantages, concrete jacketing is a practical option for the buildings where beams are highly deficient in flexure or shear as compared to the required demands.

Liew and Cheong (1991) tested the simply supported beams retrofitted with jackets by using pre-packed aggregate concrete. The additional reinforcement cage was attached by fixing the stirrups in the pre-located recesses. They concluded that the flexural strength can be predicted by assuming full bond between the existing and new concrete.

The experiments conducted by Alcocer and Jirsa (1993) on beam−column−slab sub-assemblages showed that concrete jacketing is effective in strengthening frame members including the joint region. A steel cage was provided to confine the joint core, which was effective up to a storey drift of 4%. However, the retrofitting scheme involved substantial drilling of the existing concrete.

Bhedasgaonkar and Wadekar (1995) retrofitted beams by using the expanded wire mesh reinforcement, while the supported slab was stiffened with an overlay. Cheong and MacAlevey (2000) conducted static and dynamic tests on 13 jacketed simply supported and continuous beams. The anchorage of bars was examined and negligible difference was noted, when the surface of the existing concrete was ‘partially roughened’ or ‘fully roughened’.

Shehata et al. (2009) strengthened beams by attaching the additional reinforcement using expansion bolts as shear connectors. From the test results, it was concluded that this scheme is efficient in increasing the flexural strength and stiffness of the beams.

TESTS OF BEAMS

1. Test Setup

Simply supported beam specimens are tested under a two-point loading to study the effectiveness of concrete jacketing in increasing the mid-span positive flexural capacity. The tests are also helpful in gauging the constructability of the jacketing scheme. The test setup is shown in Figure 2. An actuator is used to apply displacement controlled loading. The applied load is measured by a load cell. Linear variable differential transducers (LVDTs) are used to measure the deformations over the gauge length equal to 250 mm, i.e., the effective depth of the reference beam. This is consistent with the assumed

length of plastic hinge for the beams in the subsequent sub-assemblage specimens. Two sets of LVDTs are used on each side of the mid-span of a beam. The rotations are calculated from the deformation readings. A data acquisition system is used to record the load cell and LVDT readings.

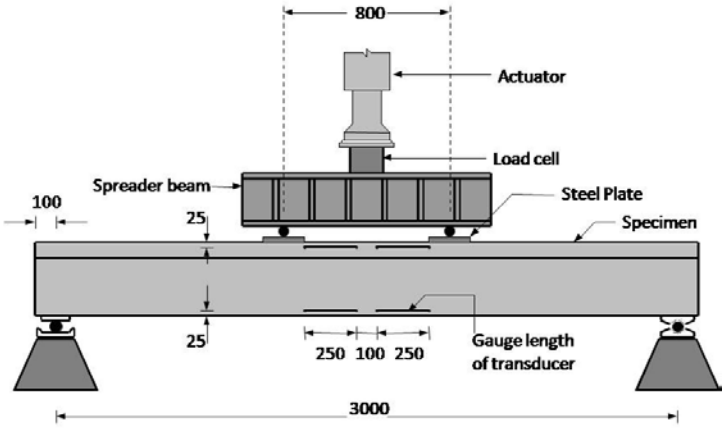

(a)

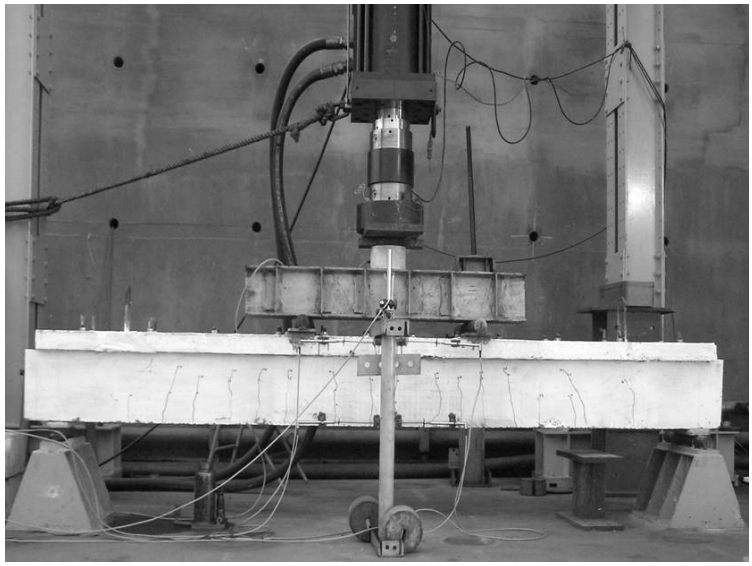

(b)

Fig. 2 Setup for testing beam specimens: (a) schematic diagram (all dimensions are in mm); (b) photograph of test setup

2. Specimen Details

2.1 Reference Specimen

A reference specimen without jacketing is tested under monotonic loading. The presence of the slab in cast-in-place beam–and–slab construction precludes the use of conventional closed stirrups. A flanged beam section is selected to simulate the obstruction due to the slab. Of course, the slab had a strengthening effect on the beams.

The sectional details of the specimen are shown in Figure 3. The material properties and reinforcement details are given in Table 1. The clear cover to the reinforcement is selected as 25 mm, since durability is not a concern in the design. The longitudinal bars are not curtailed. The stirrups at the middle third of the span are provided at a closer spacing to confine the concrete for the development of flexural plastic hinge. The concrete mix used is 1:2.35:4.65 by weight of cement, sand and coarse aggregate (of 20-mm maximum size). The water-to-cement ratio is 0.55.

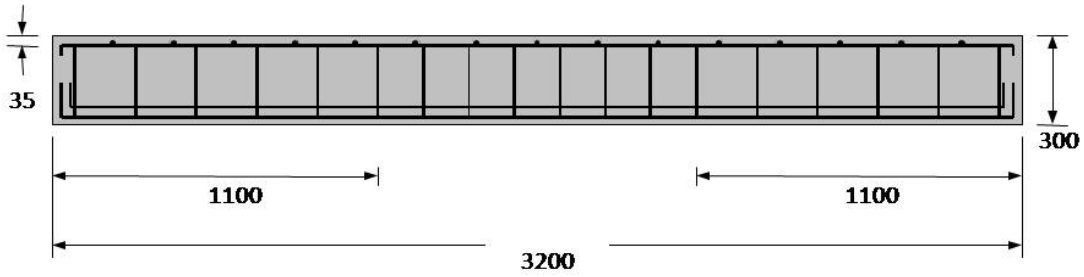

(a)

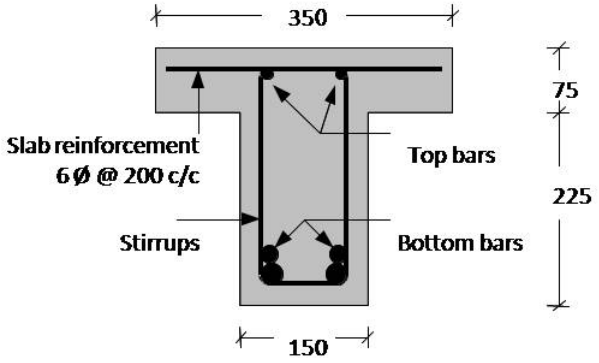

(b)

Fig. 3 Sectional details for reference beam specimen (all dimensions are in mm): (a) sectional elevation; (b) cross-section

Table 1: Material Properties and Reinforcement Details for Beam Specimens: (a) Reference Specimen; (b) Retrofitted Specimens

(a)

Specimen	Concrete	Reinforcement			Loading
	$f_{cm,E}$	Longitudinal Bars	f_y	Transverse Bars	
1	24	Top: 2-16 ϕ Bottom: 2-16 ϕ + 2-20 ϕ (p = 1.7%)	416 416 420	2 legged, 10 ϕ @ 150 c/c in the middle third of the span, and @ 175 c/c at the ends	Monotonic

(b)

Specimen	Concrete		Additional Reinforcement*		Loading
	$f_{cm,E}$	$f_{cm,J}$	Longitudinal Bottom Bars	Transverse Bars	
1	20	25	2-16 ϕ (resultant p = 1.5%)	2 legged, 8 ϕ @ 100 c/c in the middle third of the span @ 150 c/c at the ends	Monotonic
2	17	33			Cyclic

$f_{cm,E}$ = mean cube strength of existing concrete in MPa

$f_{cm,J}$ = mean cube strength of jacket concrete in MPa

f_y = yield strength of steel in MPa

ϕ = diameter of bars in mm

E = modulus of elasticity for steel (i.e., 2×10^5 N/mm^2)

p = percentage of bottom steel

*These bars are in addition to those in the existing section. The existing section has the same reinforcement as the reference specimen.

2.2 Retrofitted Specimens

Two retrofitted specimens are tested, one under each of the monotonic and half-cyclic loadings. For a retrofitted specimen, the cross-section, reinforcement detailing and the concrete mix of the inner (i.e., existing) portion are similar to the reference specimen. In jacketing a beam, the additional longitudinal bars should be limited so as to retain the ductile behaviour of the under-reinforced section. The sectional details of the specimens are shown in Figure 4. The material properties and reinforcement details are given in Table 1.

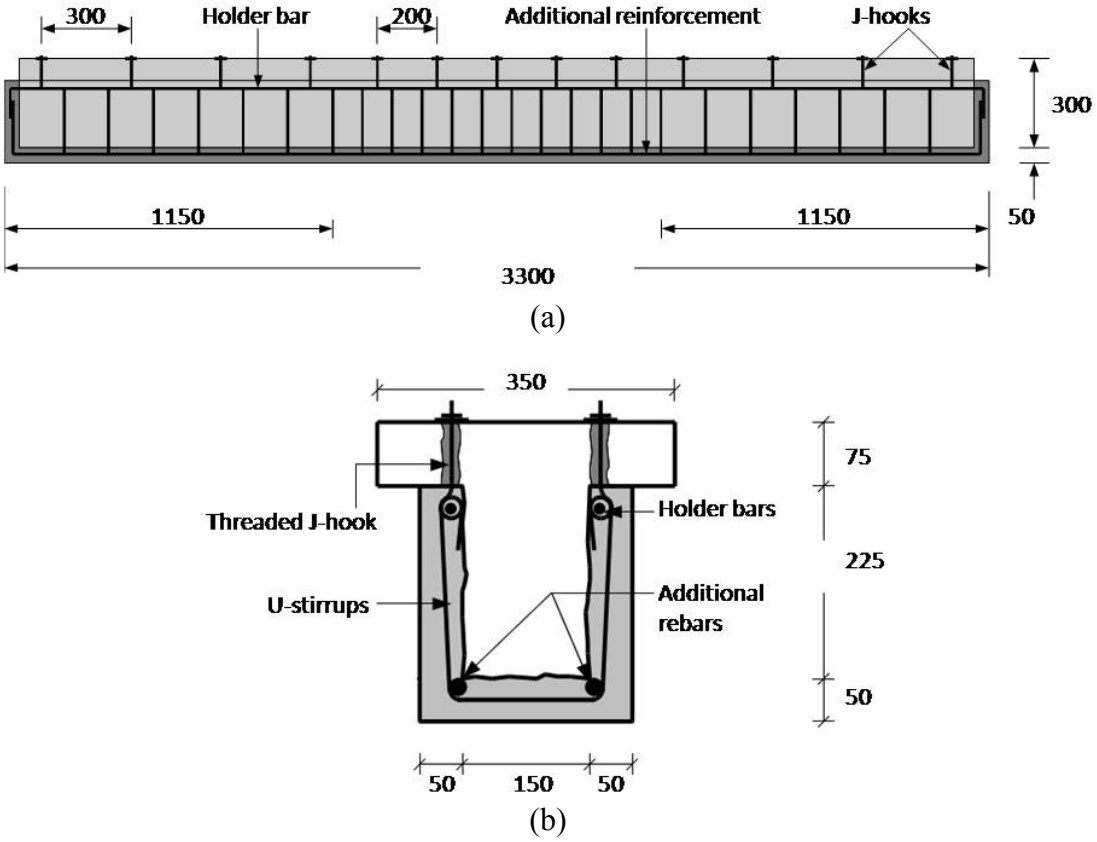

Fig. 4 Sectional details for retrofitted beam specimens (all dimensions are in mm): (a) sectional elevation; (b) cross-section

For ensuring the composite action of the jacketed beams, first the surface of the existing concrete is roughened with a motorised wire brush. The surface is cleaned with a jet of water to remove the dust. Next, the additional reinforcement cage for the jacket is anchored to the existing beam. A seismic retrofit requires closely spaced stirrups for the confinement of concrete. Drilling the slab or beam at the interval of closed stirrups can lead to considerable damage due to cracking and pop-outs. Moreover, drilling of the beam is not recommended, if the existing concrete is of poor quality. Hence, the reinforcement cage is made of open stirrups and attached to the slab by J-hooks, with holes drilled at a larger interval—in this case, at double the spacing of stirrups. The zone of compression in the beam spreads into the slab, which acts as a flange. This reduces the deficiency due to the lack of closed stirrups by delaying the crushing of concrete. The size of the J-hooks is selected such that the strength of the hooks per unit length is larger than the yield strength of the stirrups. Based on the availability, the 20-mm diameter J-hooks made of mild steel are used. Of course, the J-hooks made of high-strength steel are preferable.

The sequence of the fabrication and installation of the rebar cage is as follows:

1. Two holder bars, one for each side of the beam are passed through the eyes of two sets of J-hooks.
2. The stirrup bars are bent into the U-shape with hooked ends.
3. The stirrups are hung and secured by binding wires to the holder bars at the required spacing.
4. The required number of longitudinal bars is tied to the stirrups at the bottom corners.
5. Holes are drilled in the slab as per the spacing of the J-hooks.
6. The fabricated cage is lifted to the underside of the existing beam.

7. The threaded ends of the J-hooks are inserted through the holes drilled in the slab and are secured with nuts.

With the above technique, the reinforcement cage can be fabricated separately and then attached to the underside of an existing beam. This is convenient when applied to an existing building with high ceiling. Moreover, the technique is applicable without damaging any wall above the beam. Of course, if there is a wall beneath the beam, a few courses of masonry have to be removed to accommodate the cage. A photograph of the installed cage is shown in Figure 5.

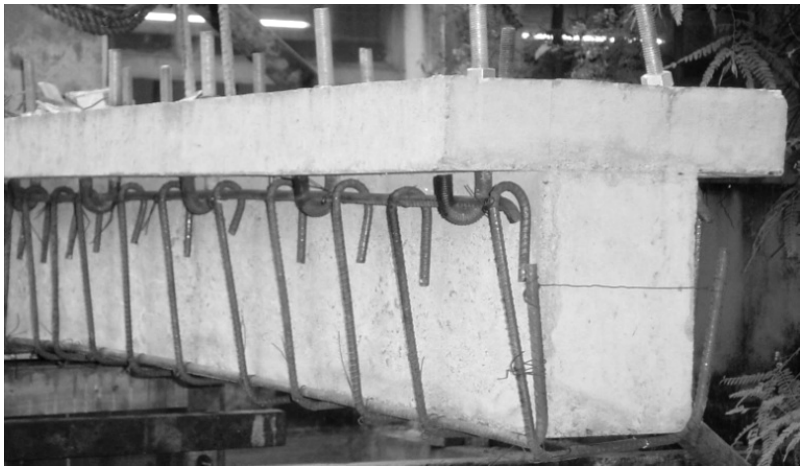

Fig. 5 Reinforcement cage for concrete jacket after installation

The jackets are made of self-compacting concrete (SCC). After several trials, a design mix of the SCC is formulated and the flowability is tested by slump flow test. Segregation of the concrete is not observed in the test.

3. Test Results

3.1 Reference Specimen

The behaviour of the specimen is found to be typical of an under-reinforced beam. The failure is characterized by well-spaced cracks in the soffit of the beam. The yielding of reinforcement is inferred from the opening of cracks and from the strain gauge readings. At each step, the rotation is calculated from the LVDT readings. An average of the two values of rotation from the two sets of LVDTs is considered.

3.2 Retrofitted Specimens

Under the monotonic loading, the behaviour of the retrofitted specimen is found to be similar to that of the reference specimen. Well-distributed flexural cracks are observed initially. Close to failure, the significant cracks are found to be localized in the middle-third region. The bottom reinforcement yields before the crushing of concrete at the top. There is no apparent delamination of the jacket up to the peak load. This is checked by light tapping with a hammer, which would reveal an air gap. Figure 6 shows the moment versus rotation curves for the reference and retrofitted specimens. The retrofitted specimen is found to have higher moment capacity with comparable ductility with respect to the reference specimen.

For the half-cyclic loading, at each displacement level, five cycles of loading are applied to study the strength and stiffness degradations. The increment of the displacement levels is taken to be the theoretical displacement corresponding to the yielding of the additional longitudinal bars. The behaviour of the specimen is characterized by a well-distributed cracking in the initial stages of loading. However, with the increasing number of cycles of loading, flexural shear cracks are observed to develop in the outer regions, in addition to the flexural cracks in the middle-third region (see Figure 7). A study of the variation of peak moment for each cycle of loading shows that the degradation of strength with the load cycles is gradual, even after reaching the flexural capacity.

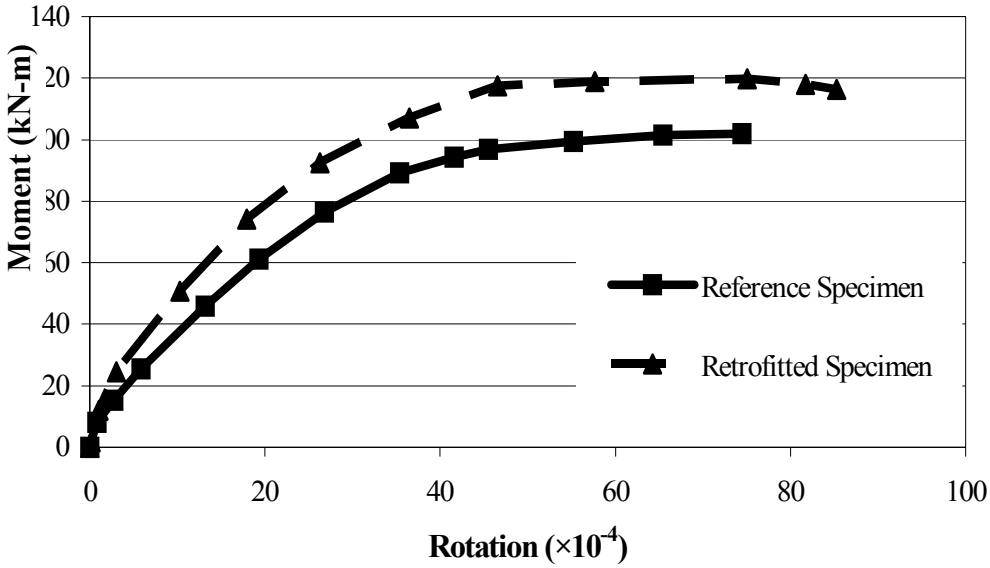

Fig. 6 Comparison of moment versus rotation curves for beam specimens tested under monotonic loading

Fig. 7 Retrofitted beam specimen during testing under half-cyclic loading

TESTS OF BEAM−COLUMN−JOINT SUB-ASSEMBLAGES

The testing of the sub-assemblages is explained in an earlier publication (Kaliyaperumal and Sengupta, 2009). However, a brief description is provided here for ready reference.

The sub-assemblage specimens were tested by using a facility that consisted of a reaction wall, a strong floor and a test frame (see Figure 8). The frame was designed and fabricated as under the present study. A specimen was erected in a steel assembly at the bottom, which had the provision of placing a hydraulic jack (for applying an upward vertical load at the bottom end of the lower column) and a vertical sliding-cum-rocking pin support. The top end of the upper column was attached to the frame through a spacer assembly and a horizontal sliding-cum-rocking bearing assembly. The lateral load was applied at the top end by an actuator fitted to the adjacent reaction wall. The ends of the beams were supported on the horizontal sliding-cum-rocking roller bearings placed on pedestals. The hold-down steel members restricted any uplift of the ends of the beams. The loads were measured by using load cells. The deformations of the beams were measured by using LVDTs near the joint, while considering a plastic hinge length equal to the effective depth of the beams of the reference specimens. The details of the test facility developed as part of this research are provided in some earlier publications (Badari Narayanan, 2010; Sengupta et al., 2006).

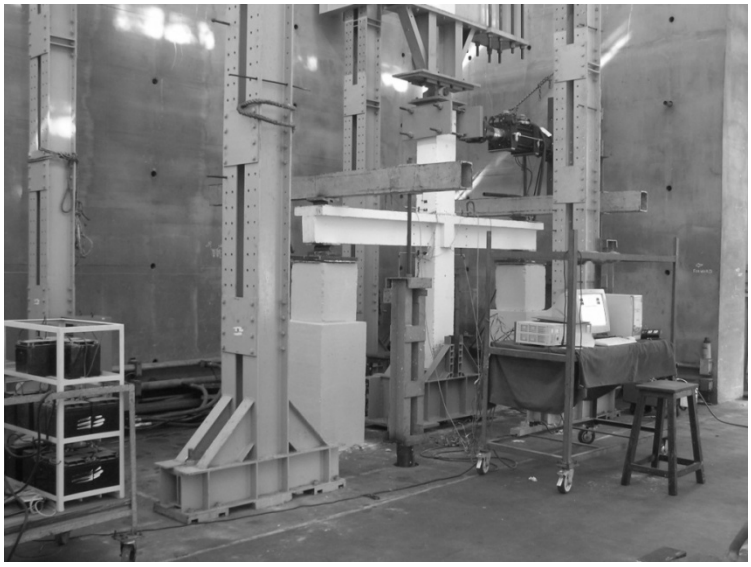

Fig. 8 Setup for testing sub-assemblage specimens

To study the lateral load versus displacement behaviour, two reference and two retrofitted specimens are tested. For each type, one specimen is tested under the monotonic lateral load and the other under the cyclic lateral load. The displacement-controlled cyclic load history is shown in Figure 9. At each displacement level, three cycles of loading are applied.

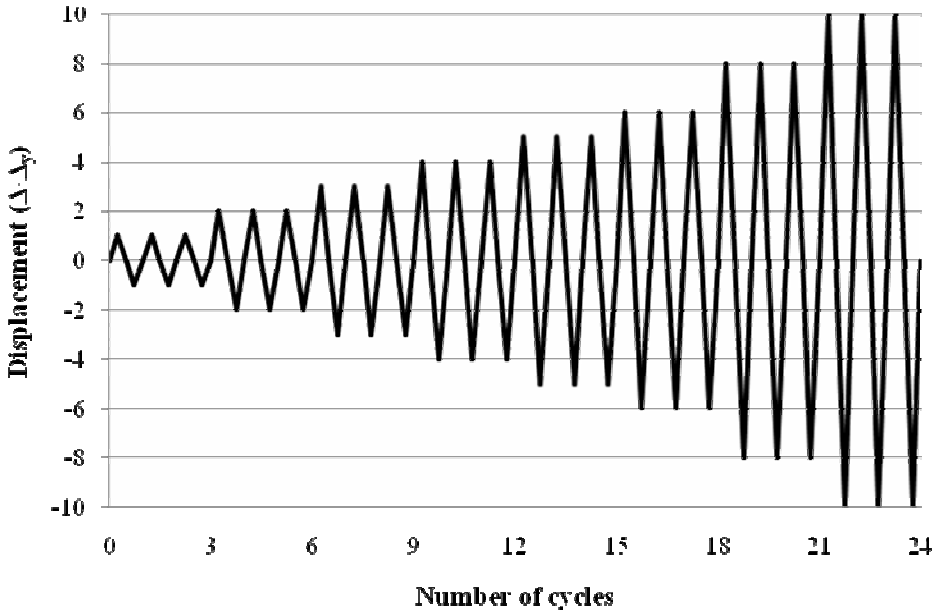

Fig. 9 Cyclic loading history

1. Specimen Details

The objective of the present study is to investigate the effects of jacketing on the positive flexural capacity of beams at the face of an interior joint. Hence, failure of the columns and shear failures of the beams or the joints are deliberately avoided. To avoid the formation of a plastic hinge in the columns prior to that in the beams, moment capacity of the columns is kept substantially higher than the moment capacity of the beams after retrofitting.

Two reference and two retrofitted specimens are tested. For each type, one specimen is tested under the monotonic and the other under the cyclic loading. The height of the specimen from the bottom pin support to the rocker pin at the top is 2.1 m. The total length of the beams between the centre-lines of the left and the right roller bearings is 3 m. Stub beams in the transverse direction and slab over the beams are

provided to create obstruction in placing the additional longitudinal and transverse bars in the jacket, like in an interior joint of an existing building.

1.1 Reference Specimens

The sectional details of a specimen are shown in Figure 10. Table 2 provides the material properties and reinforcement details for the specimens. The bottom reinforcing bars of the beam are deliberately discontinued at the joint, to simulate the conventional condition as per the gravity load design. The embedment length for the 8-mm diameter bars is selected as $L_d/3 \approx 150$ mm, where L_d is the development length in compression. Further, a concrete mix of 1:2.15:3.27 (i.e., cement:fine aggregate: coarse aggregate) proportions with a water-to-cement ratio of 0.55 is used.

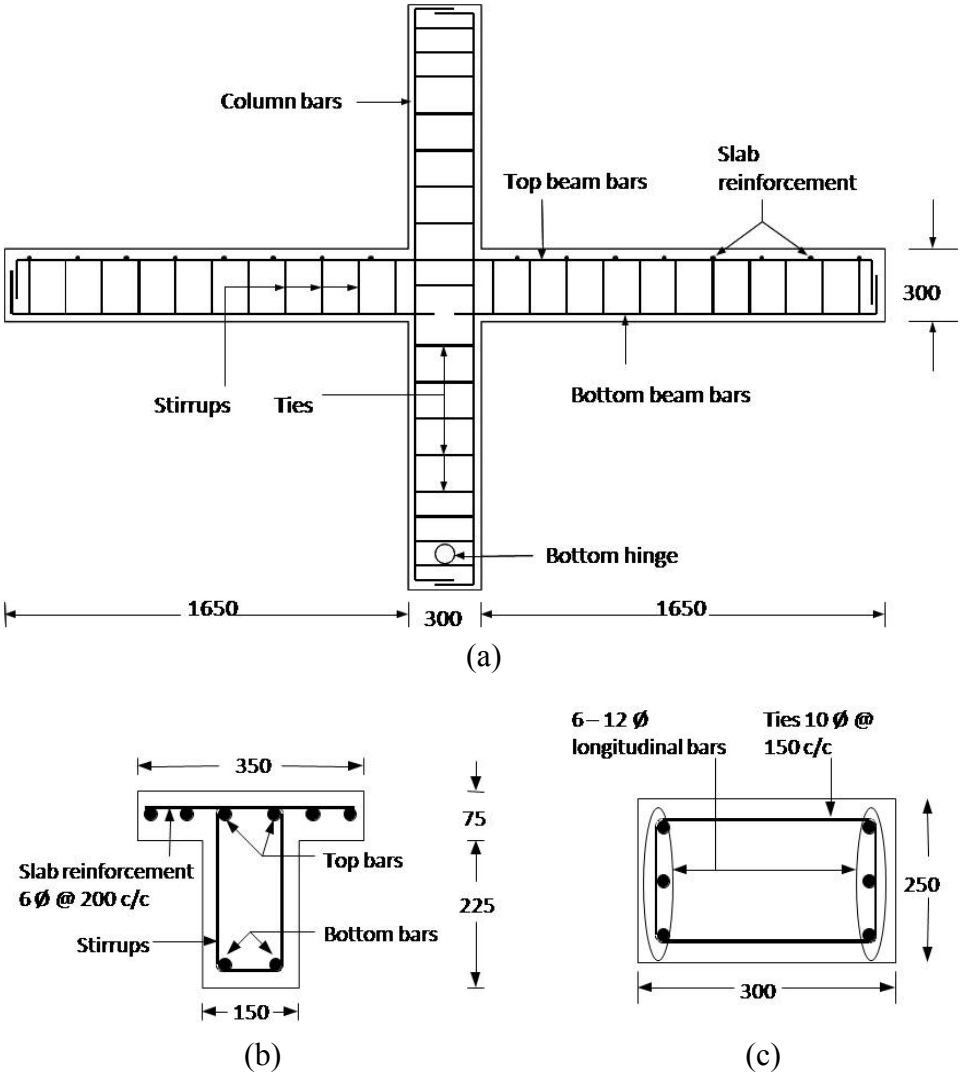

Fig. 10 Sectional details for reference sub-assemblage specimens (all dimensions are in mm): (a) sectional elevation; (b) beam section; (c) column section

1.2 Retrofitted Specimens

The details of the specimens are shown in Figure 11. The fabrication of the reinforcement for the jacket is illustrated in Figure 12. The construction procedure used for jacketing the sub-assemblage specimens is similar to that for the beam specimens. In the joint region, the additional bottom longitudinal bars are made continuous around the joint by cranking with a splay of 1 in 10. This avoids drilling through the joint. The amount of additional reinforcement is limited to ensure that the column is still stronger than the beam. The stirrups provided along the length of each splay, with spacing as per the ductile detailing requirements for a potential plastic hinge (BIS, 1993), reduce the straightening of the splay.

Table 2: Material Properties and Reinforcement Details for Sub-assemblage Specimens: (a) Reference Specimens; (b) Retrofitted Specimens

(a)

Specimen	Concrete	Reinforcement			Loading
	$f_{cm,E}$	Longitudinal Bars	f_y	Transverse Bars	
1	39	Top: 6-10 ϕ Bottom: 2-8 ϕ (p = 0.17%)	450	2 legged, 8 ϕ @ 150 c/c in the middle third of the span, and @ 200 c/c at the ends	Monotonic
2	15		420		Cyclic

(b)

Specimen	Concrete		Additional Reinforcement*		Loading
	$f_{cm,E}$	$f_{cm,J}$	Longitudinal Bottom Bars	Transverse Bars	
1	20	27	2-10 ϕ	2 legged, 8 ϕ @ 100 c/c in the middle third of the span @ 150 c/c at the ends	Monotonic
2	19	38			Cyclic

$f_{cm,E}$ = mean cube strength of existing concrete in MPa

$f_{cm,J}$ = mean cube strength of jacket concrete in MPa

f_y = yield strength of steel in MPa

ϕ = diameter of bars in mm

E = modulus of elasticity for steel (i.e., 2×10^5 N/mm^2)

p = percentage of bottom steel

*These f_y = 450 MPa bars are in addition to those in the existing section. The existing section has the same reinforcement as the reference specimen.

The additional longitudinal bars of the beams should be secured to the column reinforcement for the transfer of moment between the beams and columns in a rigid joint. In existing buildings, the column should also be jacketed to make it stronger than the jacketed beams and to satisfy the design force requirements. Hence, the columns in the specimens are also jacketed with additional longitudinal bars and ties. The slab is drilled near the four corners of the column and additional bars are continued through the holes. The additional longitudinal bars provided in the beams and columns are secured together with binding wires. Since the joints are provided with an adequate number of ties, additional confining of the joint during jacketing is not adopted. However, in a parallel study on the strengthening of columns, the joint has been confined by welding angle sections to the additional longitudinal bars for the columns (Kaliyaperumal and Sengupta, 2009).

The specimens are cast vertically to simulate the actual method of construction. The jackets of the retrofitted specimens are made of the self-compacting concrete. After the retrofit, the column jacket is flushed with the face of a transverse stub beam.

2. Test Results

For each specimen, first a constant vertical compression, approximately equal to the balanced failure load of the column in a reference specimen, is applied on the column. Next, the lateral load is applied at the top end of the upper column till the limit of the stroke length of the actuator. This is found to correspond to a drift ratio of 5.2%, where drift ratio is defined as the relative drift divided by the height between the top and bottom pins.

2.1 Reference Specimens

For the specimen tested under the monotonic lateral loading, the lateral displacement is found to be nearly zero till the load of about 10 kN. Thereafter, a sudden jump in the displacement is noticed at this load. It is inferred that this is due to the effect of friction generated at the sliding bearing in the presence of the vertical load. The first few cracks near the joint, at the soffit of the beam undergoing sagging and at

the slab undergoing hogging, are found to be dispersed. Close to the peak lateral load, single major cracks are observed on both sides of the joint (see Figure 13(a)). Even though the bottom longitudinal bars in the beams are discontinuous at the joint, an appreciable pull-out of the bars is not observed. This is because a small diameter of the bars generates good bond and the axial compression through the column enhances this bond. At the peak load, the lateral drift at the top is about 20 mm and the corresponding drift ratio is 0.95%.

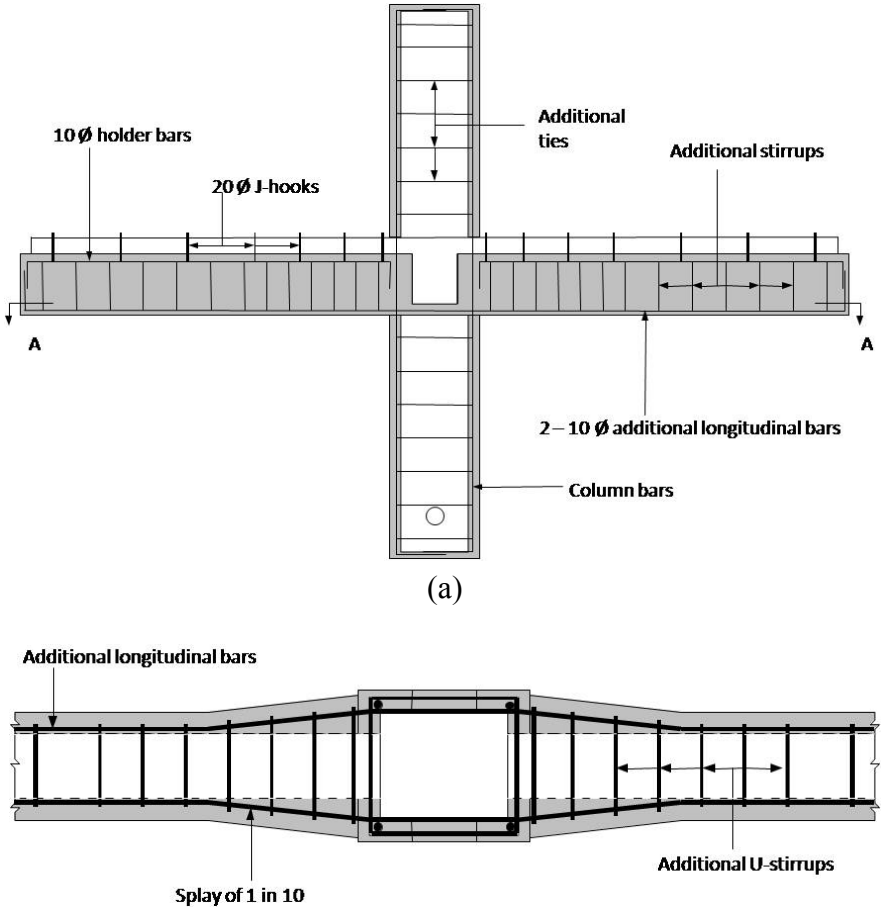

Fig. 11 Sectional details for retrofitted sub-assemblage specimens: (a) sectional elevation, (b) section A-A

Fig. 12 Fabrication of reinforcement for retrofitted sub-assemblage specimens

For the specimen tested under the cyclic lateral loading, the spalling of the cover concrete and pull-out of the bottom bars is observed after several cycles of loading. Vertical cracks are found to form on the

top of the slab due to hogging. A horizontal crack is found to propagate towards the joint at the level of the top reinforcement, thus showing the degeneration of bond and yield penetration into the joint (see Figure 13(b)).

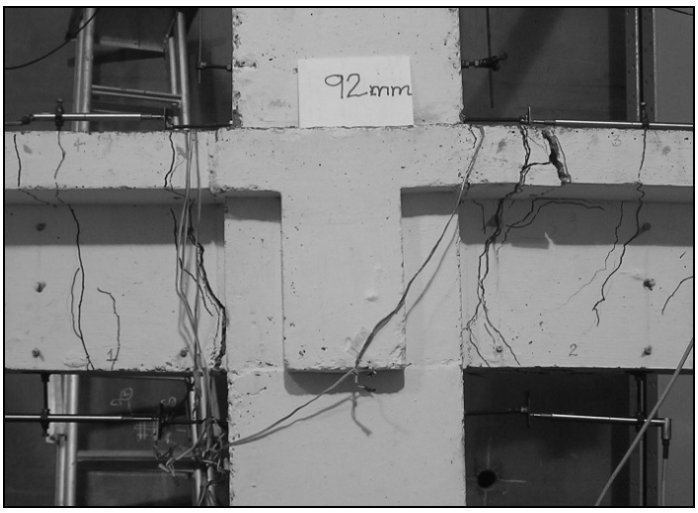

(a)

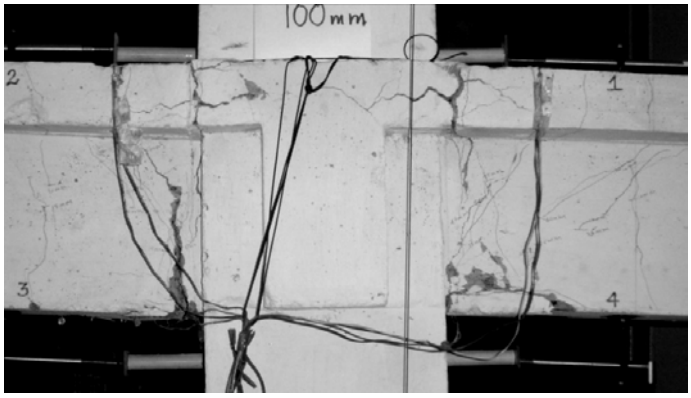

(b)

Fig. 13 Close-up view of reference sub-assemblage specimens during testing under: (a) monotonic loading; (b) cyclic loading

2.2 Retrofitted Specimens

The behaviour of the retrofitted specimen tested under the monotonic loading is similar to that of the reference specimen. No spalling of concrete or buckling of the additional longitudinal bars is observed throughout the experiment. The failure of beams is characterized by the formation of major cracks at the faces of the original joint (see Figure 14(a)). The crack-width is large due to the yielding of the longitudinal bars of the beams. The portion of the jacket concrete around the corners of the joint is found to be delaminated. At the peak load, the observed lateral drift at the top is about 42 mm and the corresponding drift ratio is 1.9%.

The retrofitted specimen tested under the cyclic loading is found to behave satisfactorily with regard to strength and ductility without any premature failure, such as buckling of the longitudinal bars or delamination of the jacket (see Figure 14(b)). However, the pinching effect is not found to be reduced.

The lateral load versus sagging rotation curves for the reference and retrofitted specimens tested under the monotonic loading are compared in Figure 15. The lateral load capacity of the retrofitted specimen shows improvement compared to that of the reference specimen. Although the stiffness of the retrofitted specimen is affected by the jacketing of the column, the strength is primarily governed by the attaining of the positive flexural capacity of the retrofitted beams.

(a)

(b)

Fig. 14 Close-up view of retrofitted sub-assemblage specimens during testing under: (a) monotonic loading; (b) cyclic loading

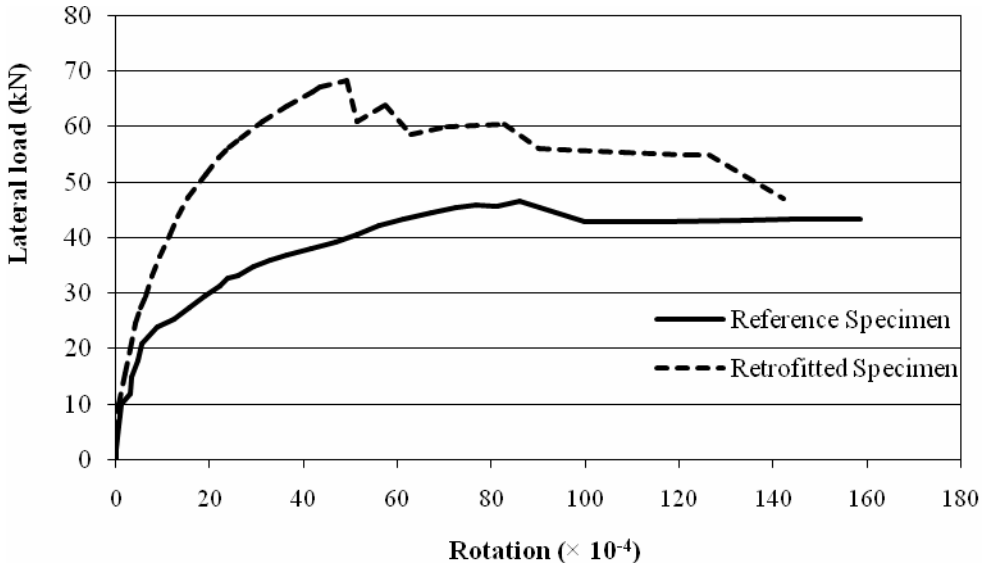

Fig. 15 Comparison of lateral load versus sagging rotation curves for the sub-assemblage specimens tested under monotonic loading

The lateral load versus displacement curves for the reference and retrofitted specimens tested under the cyclic loading are compared in Figure 16. It may be observed that there is an increase in the lateral strength after retrofitting. Also, there is an increase in the energy dissipation. However, the pinching of

the hysteresis loops is not improved. This possibly happens as the yielding of longitudinal bars in the beams leads to a wide opening of cracks.

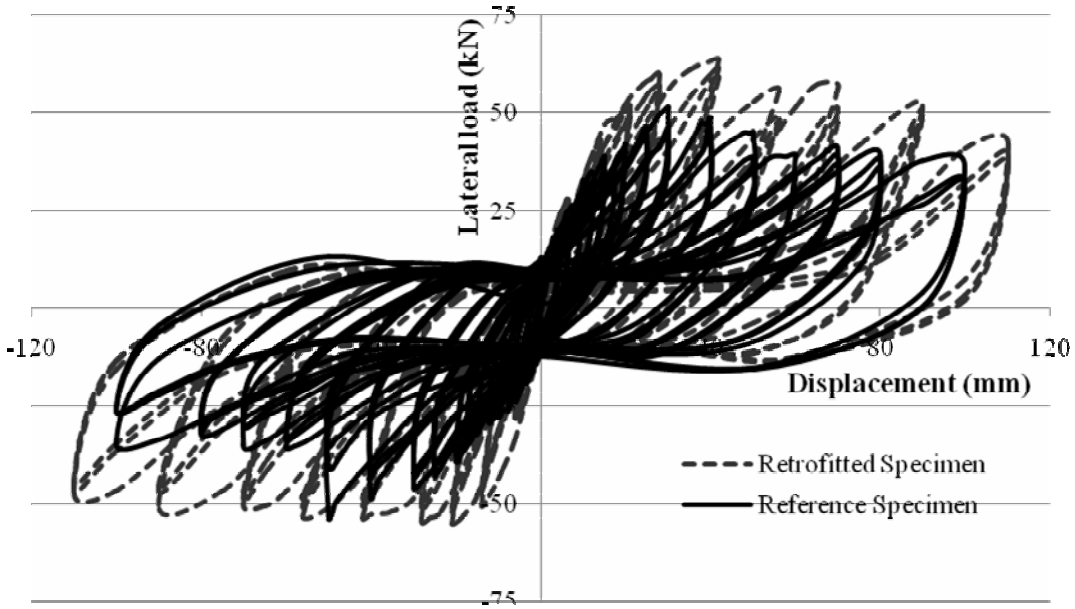

Fig. 16 Comparison of lateral load versus displacement curves for the sub-assemblage specimens tested under cyclic loading

2.3 Comparison of Monotonic and Cyclic Tests

The lateral load versus displacement curves for the monotonic and cyclic loadings of the reference specimen are overlapped in Figure 17. The corresponding curves for the retrofitted specimens are shown in Figure 18. For both the reference and retrofitted specimens, the monotonic tests are found to provide sufficiently good estimates of the envelope behaviour of the lateral load versus displacement curves obtained under the cyclic loading. Hence, the values of strength and ductility, as calculated from the lateral load versus displacement curves obtained under the monotonic loading, may be considered to be rational estimates for the cyclic loading. Of course, energy dissipation can be estimated only from the cyclic test.

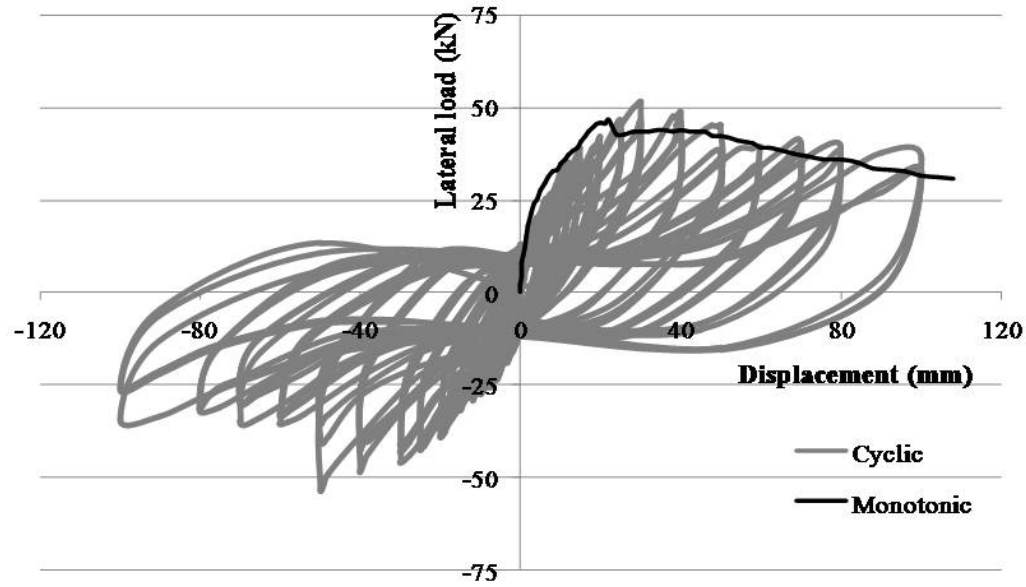

Fig. 17 Comparison of lateral load versus displacement curves for the reference sub-assemblage specimens tested under monotonic and cyclic loadings

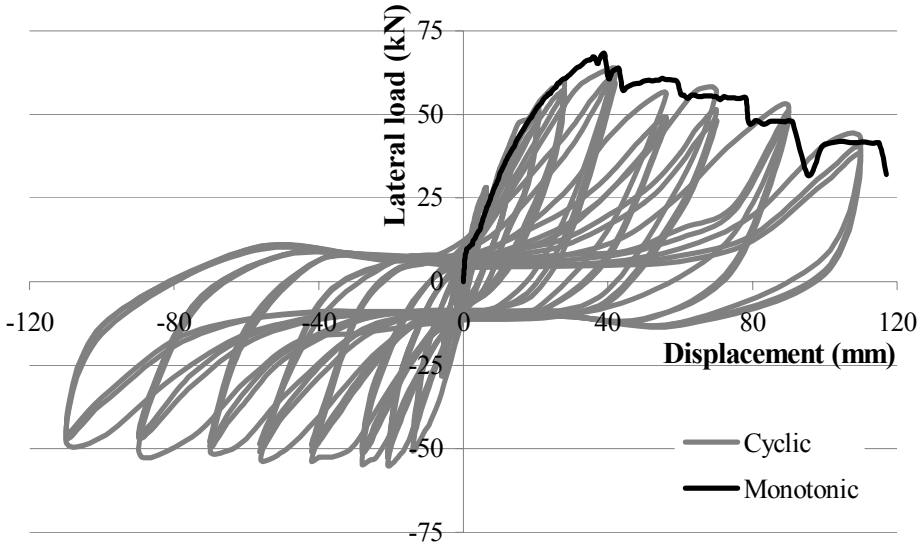

Fig. 18 Comparison of lateral load versus displacement curves for the retrofitted sub-assemblage specimens tested under monotonic and cyclic loadings

2.4 Observations

Following observations are made from the beam–column–joint sub-assemblage tests:

1. The retrofitted specimens do not show any apparent delamination between the existing concrete and the concrete in the jacket.
2. The lateral load capacity of the retrofitted specimen tested under the monotonic loading is 1.46 times that of the reference specimen.
3. The lateral load capacity of the retrofitted specimen tested under the cyclic loading is 1.23 times that of the reference specimen.
4. Under the cyclic loading, the cumulative energy dissipated till the attaining of the peak load (at a displacement of 42 mm) for the retrofitted specimen is 14285 kN-mm, as against 12697 kN-mm for the reference specimen (at the same displacement).

ANALYSIS OF RETROFITTED SECTIONS

The moment versus rotation curves for the retrofitted sections are predicted by the layered (or lamellar) analysis approach. Although this approach is well established for heterogeneous sections, the objective of the present analysis is to investigate its applicability for a retrofitted section in a member under predominantly flexural deformations. A simplified analysis considering a uniform grade of concrete is compared with the rigorous analysis, as the simplified analysis may be more suitable for professional practice.

First, the behaviour of the retrofitted beam specimen tested under the monotonic loading is predicted. Next, the predicted behaviour of the beams near the joint is used to estimate the lateral load versus displacement behaviour of the retrofitted sub-assemblage specimen tested under the monotonic loading.

1. Layered Analysis

A retrofitted section is a heterogeneous section with two grades of concrete and several layers of reinforcement bars. To account for the heterogeneity, a layered method of analysis is used, wherein the section is divided into layers through the depth. For the concrete under compression, the parabolic-plastic stress versus strain model, as given in IS 456 (BIS, 2000), is used for the existing concrete as well as the concrete for the jacket, with the corresponding strengths as given in Tables 1 and 2. Any confinement of the existing concrete is neglected as closed stirrups are not used in the jacket. A perfect bond for the strain compatibility between the existing concrete and the jacket is assumed. For concrete under tension, the effect of tension stiffening is considered by using the stress versus strain model proposed by Kaklauskas and Ghaboussi (2001). For the steel bars, an elasto-plastic stress versus strain model is adopted. For a sub-assemblage specimen, the tensile strength of the discontinuous bottom bars in a beam is reduced based on the provided embedment length.

2. Simplified Analysis

The simplified analysis is based on a uniform concrete strength (which is same as that of the existing concrete) throughout the section. The tension stiffening effect of concrete is neglected.

3. Results for the Beam Specimen

Figure 19 shows the comparison of the theoretical predictions with the test results of the moment versus rotation behaviour at the central region for the retrofitted beam tested under the monotonic loading. The test results show a higher stiffness for the beam than that predicted, in the initial stages from the cracking of concrete up to the yielding of the bars. Thus, the tension stiffening is underestimated in the layered analysis. Of course, this effect is significant only up to the yielding of the bars. Beyond that, there is a good agreement between the experimental and theoretical curves. The observed flexural capacity of the specimen is only 4% less than that predicted. The ductilities shown by the two curves are comparable. Hence, it is concluded that there is no slippage between the concrete layers, and the scheme selected for retrofitting is effective in increasing the positive flexural capacity while retaining the ductility.

There is little or no difference between the results of the layered and the simplified analyses. This is because the thickness of the jacket is small and the compressive strengths of the two grades of concrete are not widely different.

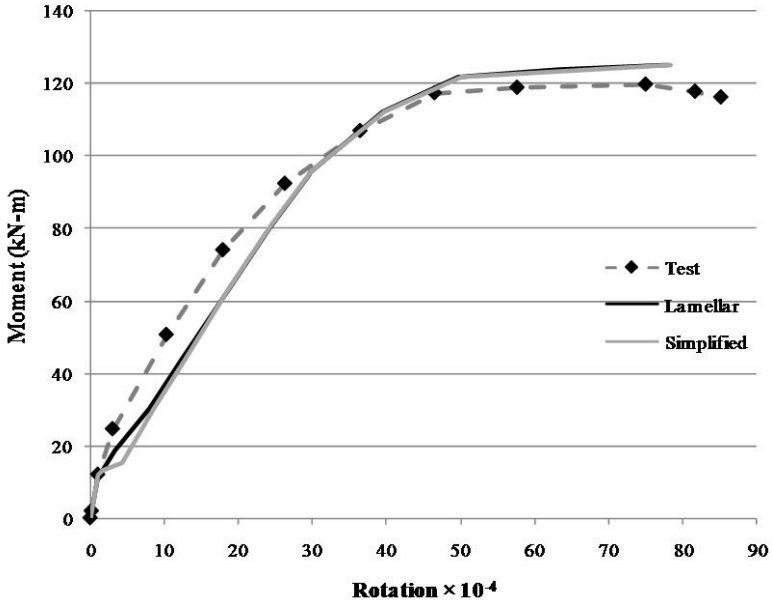

Fig. 19 Comparison of moment versus rotation curves for the retrofitted beam specimen tested under monotonic loading

4. Results for the Sub-assemblage Specimen

The lateral load versus displacement curve for the retrofitted specimen tested under the monotonic lateral loading is predicted by a computational model of the sub-assemblage. Initially, a conventional pushover analysis is conducted by assigning bilinear moment versus rotation properties (up to the peak) for the lumped plastic hinges in the beams at the faces of the joint. It is observed that the nonlinearity in the overall behaviour could not be predicted with sufficient accuracy. Next, an incremental nonlinear analysis is conducted by considering spread plasticity and by varying flexural stiffness for the plastic hinge regions of the beams. The method of analysis used here is explained in an earlier publication (Kaliyaperumal and Sengupta, 2009). Only a brief description is provided below for ready reference.

The computational model for the sub-assemblage developed by using frame elements and appropriate boundary conditions is shown in Figure 20. To consider spread plasticity, the beam members are sub-divided for isolating the plastic hinge regions of length 250 mm (which is approximately equal to the effective depths of the beams) from the faces of the joint. Next, at each step of the lateral load P_{Hi}, the secant flexural stiffness values, based on the predicted moment versus rotation curves from a layered analysis of the beam section under sagging and hogging, are assigned to the plastic-hinge elements. Next,

a linear analysis is performed to get the lateral displacement Δ_i at the top end of the upper column due to P_{Hi}. The $P-\Delta$ effect due to the displacement of the vertical load P_V at the top end of the upper column is included. The analysis is conducted for the incremental values of P_{Hi}.

In the experiments, horizontal frictional forces are induced at the bearings, at the ends of the beams and at the top end of the upper column, due to the reactions from the axial load. The frictional forces increase the stiffness of the experimental lateral load versus displacement curve. For a precise prediction of this behaviour, it is decided to include the frictional forces in the computational model. First, the bearings are tested to determine their coefficients of friction. From the tests, it is found that the roller bearings at the beam ends have the coefficient of friction μ_r equal to 0.11. The coefficient of friction for the bearing assembly at the top of the column, μ_s, is 0.035. Next, a frictional force at a bearing is calculated by multiplying the vertical reaction at the bearing, corresponding to a load step, with the coefficient of friction. The value of each vertical reaction is calculated from statics due to P_V or P_H or both.

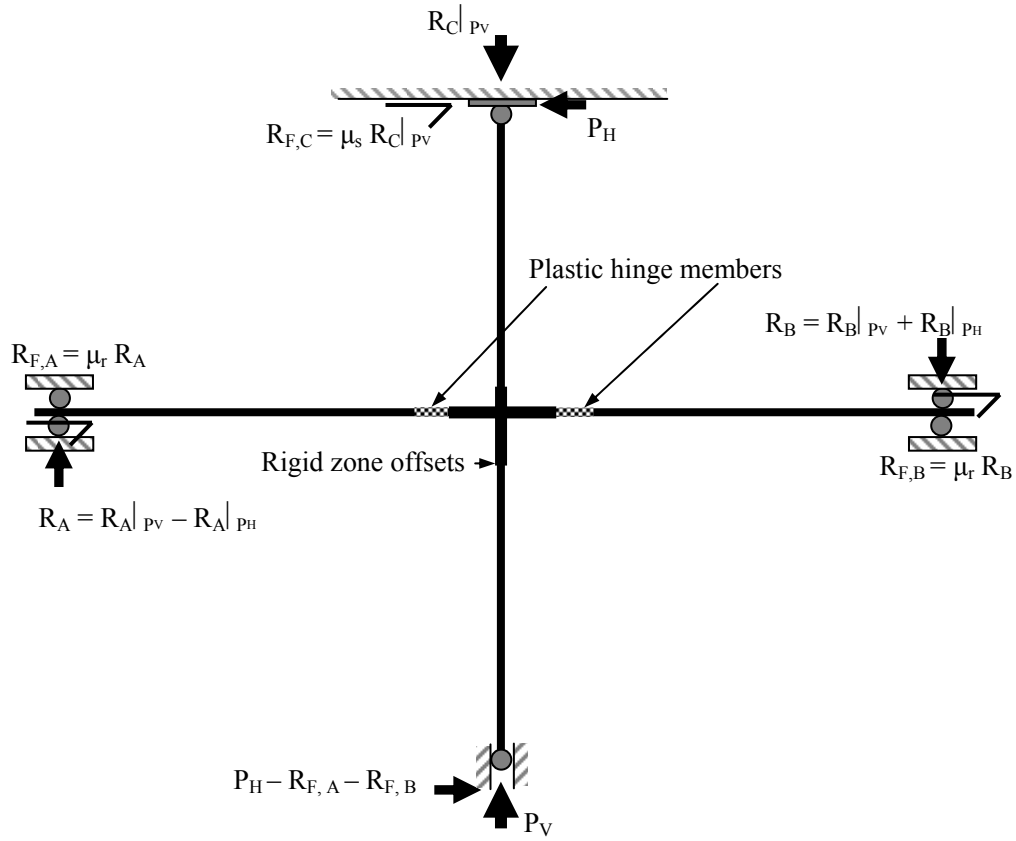

Fig. 20 Computational model for a sub-assemblage specimen

From the incremental nonlinear analysis, the predicted lateral load versus displacement curve for the retrofitted specimen tested under the monotonic lateral loading is plotted in Figure 21. It can be observed that the predicted curve is close to the experimental results almost up to the peak. Near the peak, the experimental results deviate from the predicted curve due to the widening of the cracks in the jacket at the corners of the joint.

GUIDELINES FOR PROFESSIONAL PRACTICE

1. Analysis of Retrofitted Sections

A layered analysis can be adopted for a retrofitted section considering different strengths and behaviour of the existing concrete and the concrete in the jacket. A preloaded section can be analyzed by considering initial strain in the existing section. Neglecting slippage, the strain differences at the interface

of the two concrete should be maintained to satisfy the strain compatibility. A simplified analysis considering a uniform compressive strength (equal to that of the lower-grade concrete) throughout the section can be adopted for quick calculations.

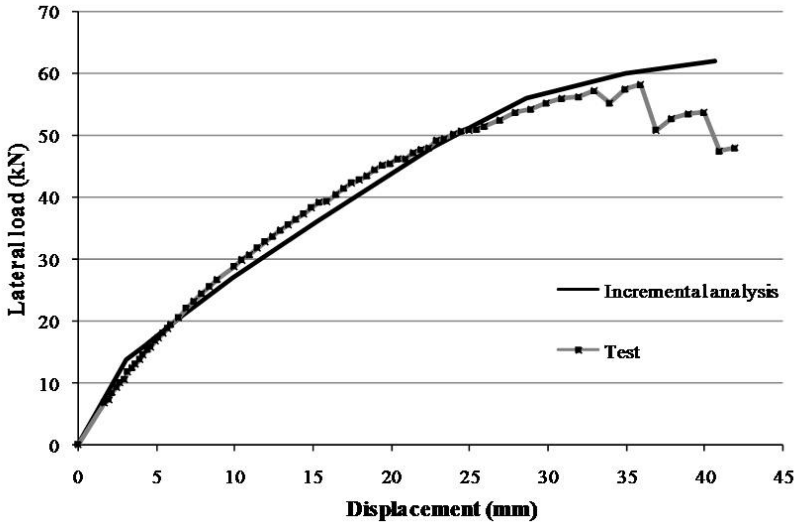

Fig. 21 Comparison of lateral load versus displacement curves for the retrofitted sub-assemblage tested under monotonic loading

2. Design of Additional Bars for a Beam

- The required additional longitudinal bars for a beam are to be calculated based on the moment demand from the worst combination of gravity and seismic loads. However, the amount of additional reinforcement should be limited to ensure that the supporting column is still stronger than the beams.
- The additional stirrups and their spacing are to be calculated based on the shear demand from the capacity-based design expression and the requirement of confinement (BIS, 1993). This is to ensure the ductile detailing of the potential plastic-hinge regions.

3. Detailing

- In order to avoid any damage in the primary frame members made of poor concrete, the drilling of holes should be minimized in selecting a scheme of reinforcement for the concrete jacket. The additional longitudinal bars (that may be bundled, if required) can be placed near the corners of the beam and cranked around the joint with a splay of 1 in 10 or higher. This will avoid drilling holes through the joint. Although stirrups are provided along the length of the splay, at the spacing required for a potential plastic hinge, extra stirrups should be provided at the beginning of the splay (i.e., at the narrower section) to reduce the tendency of straightening of the bars and consequent breaking of the jacket concrete. A similar scheme may be adopted for the transverse beam, if retrofitted. The bars are to be tied with the added longitudinal bars in the column for the transfer of moment.
- The splaying of the bars and the jacket may not be architecturally acceptable for a column sufficiently wider than the beam. In such a case, drilling through the joint may be inevitable. However, this should be done with caution, since drilling reduces the shear capacity of the joint and may damage some existing bars in the column.
- The additional stirrups can be made of U-shaped bars to avoid drilling of the beams. The bars with end hooks can be hung and secured by binding wires to a holder bar on each side of the web of a beam. Alternately, they can be welded to the holder bars, provided weldable bars are used. The holder bars can be attached to the slab above the beam by J-hooks and nuts at a suitable interval.
- The additional stirrups can be closed (by using lapped U-bars and drilling through the slab) for an improved confinement, provided the existing concrete is of good quality and the drilling is executed carefully.
- If a building was not designed for the seismic forces, it is expected that the columns are inadequate in terms of flexural and shear capacities. The joints may also not have adequate shear capacity. The proposed detailing considers these factors along with the possible deficiency in the positive flexural

capacity of the beam. The columns should also be jacketed with additional reinforcement for maintaining a strong-column-weak-beam design. The joint can be confined by welding angle sections to the additional longitudinal bars in the columns. The details of column jacketing and strengthening of joints are illustrated in Kaliyaperumal and Sengupta (2009).

- For a beam wider than 300 mm, distributed longitudinal bars across the soffit should be provided. These bars are not continuous at the joint. However, they should be anchored to the added ties of the column with end hooks. For a beam with a large depth, additional side-face reinforcement can be provided as per the conventional design.
- A minimum cover should be provided as per IS 456 (BIS, 2000) to satisfy the fire safety and durability requirements.

4. Construction

- If possible, a beam should be subjected to reduced service loads before the casting of the jacket. The slab can be supported on the props adjacent to the beam.
- After chipping any plaster, the surface of the existing concrete should be roughened without damaging the concrete, especially in the case of poor quality of existing concrete. Hence, roughening by a motorised wire brush is preferred to hacking. To avoid the weakness of a cold joint, sand blasting the surface can provide more roughness by exposing the aggregates. Holes are drilled in the slab as per the spacing of the J-hooks (see Figure 22(a)).
- The surface should be thoroughly cleaned with a jet of water to remove the dust and wetted before jacketing.
- The new reinforcement cage can be fabricated at the floor beneath, lifted to the underside of the beam, and attached to the slab by J-hooks and nuts (see Figures 22(b) and 22(c)). The additional longitudinal bars and ties for the column are then placed. The longitudinal bars are continuous through the slab and welded with angle sections near the joint. They are tied with the additional longitudinal bars for the beam.
- Self-compacting concrete (SCC) or shotcrete can be used for the jacket. The flowability of SCC is important with regard to the filling up of the annular space between the existing concrete and the formwork. A shrinkage-compensating admixture needs to be added in the new concrete.
- The concrete jacket should be adequately cured before the beam is reloaded.

SUMMARY AND CONCLUSIONS

The present study has investigated the effect of jacketing on the positive flexural capacity and performance of beams near an interior joint. First, the testing of the reference and retrofitted simply supported beam specimens under a two-point bending has been documented. Second, the testing of the beam-column-joint sub-assemblage specimens has been explained. Third, the prediction of the strength and behaviour of the retrofitted beam specimens has been illustrated. A layered analysis and a simplified analysis have been used for the predictions. The incremental nonlinear analysis for predicting the lateral load versus displacement behaviour of a sub-assemblage has been highlighted. Finally, guidelines have been provided for the retrofitting of beams by concrete jacketing.

Following conclusions have been obtained from the present study:

- From the beam tests, it has been observed that the increase in strength and retention of ductility after concrete jacketing is as predicted by the analysis.
- The retrofitted specimens do not show a visible delamination between the existing concrete and the concrete in the jacket. The roughening of the surface of the existing concrete by motorised wire brush has been found to be satisfactory for the type of tests conducted.
- For the selected scheme of jacketing, the retrofitted sub-assemblage tested under the monotonic loading has shown expected increase in the lateral strength. The ductility after retrofitting is found to be adequate.
- The degradations of the strength and stiffness of the retrofitted sub-assemblage under the cyclic loading are gradual. Energy dissipation increases after the retrofitting. However, pinching in the hysteresis loops cannot be reduced.
- A layered analysis provides a good prediction of the strength and the moment versus rotation behaviour of a retrofitted section. The simplified analysis is also sufficiently accurate.

- The prediction of the lateral load versus displacement behaviour of a sub-assemblage, by a conventional pushover analysis based on a bilinear (up to the peak) moment versus rotation curve for a lumped plastic hinge, is approximate, especially in the pre-yield region.
- The incremental nonlinear analysis with varying flexural stiffness for the hinge members (to model the spread plasticity), and incorporating friction of the bearings, has shown a substantially better prediction of the lateral load versus displacement behaviour of the retrofitted sub-assemblage specimen as compared to the conventional pushover analysis.

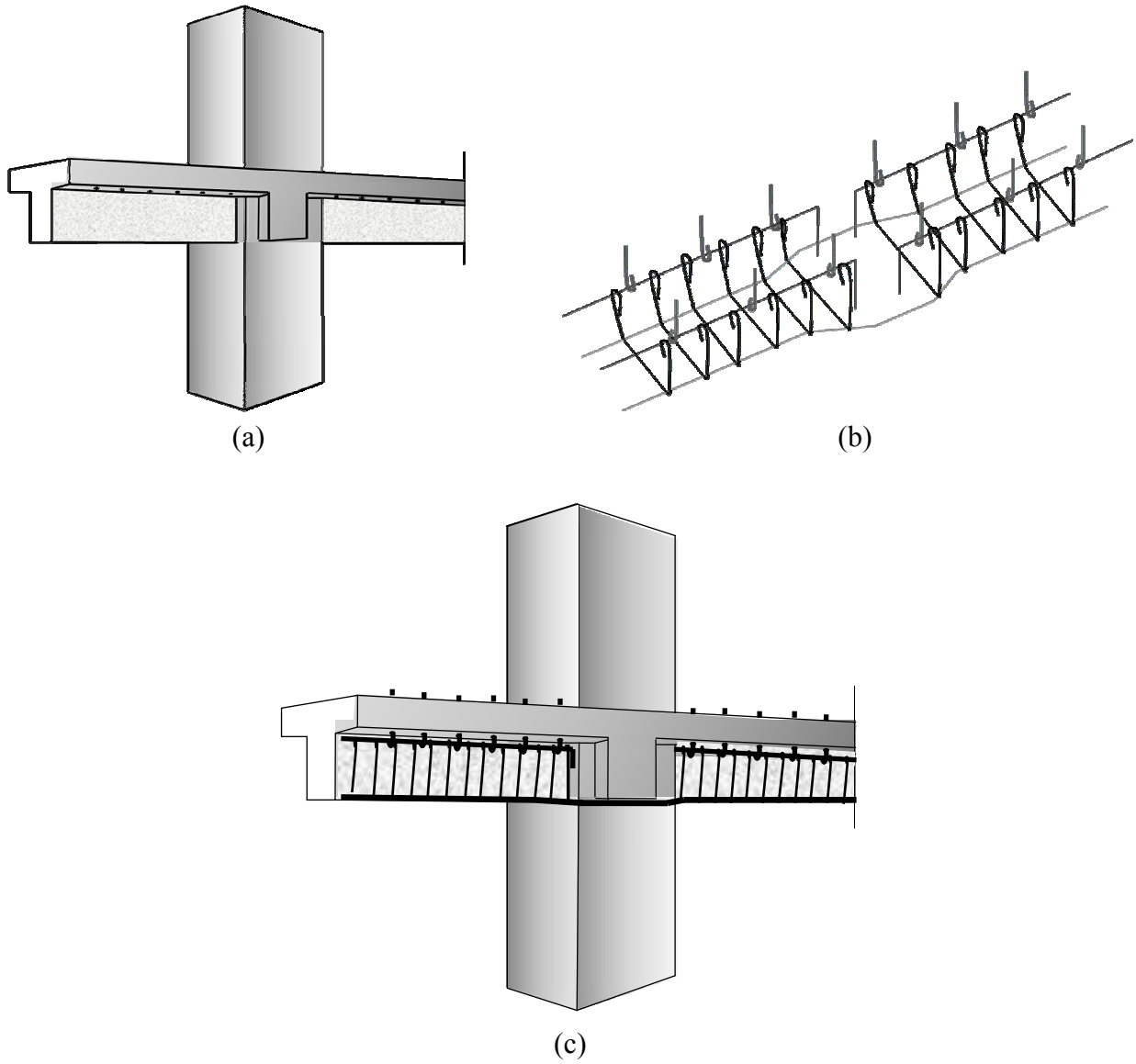

Fig. 22 Scheme of jacketing for enhancing positive flexural capacity of a beam near an interior joint (column bars not shown for clarity): (a) drilling of holes and surface preparation; (b) fabrication of reinforcement cage; (c) installation of reinforcement cage

The scheme of concrete jacketing selected in the present study needs to be qualified under a fast cyclic loading. Under this type of loading, the bond of the reinforcing bars deteriorates, leading to a drop in the strength. This study can be extended to the exterior beam−column joints by testing the corresponding sub-assemblage specimens retrofitted with a suitable jacketing scheme. The strengthening of beams for shear also needs to be studied, especially on considering the high percentage of shear deficiencies of beams in the existing buildings. Three-dimensional frames with jacketed members can be tested under monotonic or cyclic lateral loads or base excitation applied by using a shake table.

ACKNOWLEDGEMENTS

The funding from the Centre for Industrial Consultancy and Sponsored Research, Indian Institute of Technology Madras, and the Fund for Improvement of Science and Technology Infrastructure (FIST) grant from the Government of India, are gratefully acknowledged.

REFERENCES

1. Alcocer, S.M. and Jirsa, J.O. (1993). "Strength of Reinforced Concrete Frame Connections Rehabilitated by Jacketing", ACI Structural Journal, Vol. 90, No. 3, pp. 249–261.
2. Badari Narayanan, V.T. (2010). "Seismic Retrofit of Reinforced Concrete Beams in Buildings for Sagging Moment Using Concrete Jacket", Ph.D. Thesis, Department of Civil Engineering, Indian Institute of Technology Madras, Chennai.
3. Bhedasgaonkar, B.V. and Wadekar, M.K. (1995). "Repairs of Beams and Slab with Excessive Deflection", The Indian Concrete Journal, Vol. 69, No. 1, pp. 47–50.
4. BIS (1993). "IS 13920: 1993—Indian Standard Ductile Detailing of Reinforced Concrete Structures Subjected to Seismic Forces—Code of Practice", Bureau of Indian Standards, New Delhi.
5. BIS (2000). "IS 456: 2000—Indian Standard Plain and Reinforced Concrete—Code of Practice (Fourth Revision)", Bureau of Indian Standards, New Delhi.
6. Chakrabarti, A., Menon, D. and Sengupta, A.K. (editors) (2008). "Handbook on Seismic Retrofit of Buildings", Alpha Science International Ltd., Oxford, U.K.
7. Cheong, H.K. and MacAlevey, N. (2000). "Experimental Behavior of Jacketed Reinforced Concrete Beams", Journal of Structural Engineering, ASCE, Vol. 126, No. 6, pp. 692–699.
8. Kaklauskas, G. and Ghaboussi, J. (2001), "Stress-Strain Relations for Cracked Tensile Concrete from RC Beam Tests", Journal of Structural Engineering, ASCE, Vol. 127, No. 1, pp. 64–73.
9. Kaliyaperumal, G. and Sengupta, A.K. (2009). "Seismic Retrofit of Columns in Buildings for Flexure Using Concrete Jacket", ISET Journal of Earthquake Technology, Vol. 46, No. 2, pp. 77–107.
10. Liew, S.C. and Cheong, H.K. (1991). "Flexural Behavior of Jacketed RC Beams", Concrete International, Vol. 13, No. 12, pp. 43–47.
11. Murty, C.V.R., Goel, R.K., Goyal, A., Jain, S.K., Sinha, R., Rai, D.C., Arlekar, J.N. and Metzger, R. (2002). "Reinforced Concrete Structures", Earthquake Spectra, Vol. 18, No. S1, pp. 149–185.
12. Sengupta, A.K., Satish Kumar, S.R., Badari Narayanan, V.T. and Gnanasekaran, K. (2006). "Facility for Testing Beam-Column Sub-assemblages", Proceedings of the 13th Symposium on Earthquake Engineering, Roorkee, pp. 925–933.
13. Shehata, I.A.E.M., Shehata, L.C.D., Santos, E.W.F. and Simões, M.L.F. (2009). "Strengthening of Reinforced Concrete Beams in Flexure by Partial Jacketing", Materials and Structures, Vol. 42, No. 4, pp. 495–504.

ISET Journal of Earthquake Technology, Paper No. 519, Vol. 49, No. 1-2, March-June 2012, pp. 23–35

NN-BASED DAMAGE DETECTION IN MULTI-STOREY BUILDINGS FROM MODAL PARAMETER CHANGES

Hemant Kumar Vinayak*, Ashok Kumar**, Pankaj Agarwal** and Shashi Kant Thakkar**
*Department of Civil Engineering
National Institute of Technology Hamirpur, Hamirpur-177005
**Department of Earthquake Engineering
Indian Institute of Technology Roorkee, Roorkee-247667

ABSTRACT

To determine the relative status of the damaged floors of a building after an earthquake by using modal characteristics of the building, instrumentation of the building is not required throughout its lifetime. In this paper, the accuracy of neural networks trained with fractional frequency and mode shape changes, as obtained from the combinations of three, four and five damage levels of different storeys of the building, is evaluated. The networks trained with a combination of three damage levels are found to be incapable of giving acceptable results in the case of four- and eight-storey buildings considered. However, for the four-storey building, the networks trained with four damage levels predict good results and the networks trained with five damage levels predict excellent results. For the eight-storied building, the networks trained with four damage levels give acceptable results for storey level damage. Further, the accuracy of damage severity is found to decrease with an increase in the number of building storeys.

KEYWORDS: Damage Detection, Neural Network, Frequency, Mode Shape, Stiffness

INTRODUCTION

The need to interpret correlation between input and output values, which do not have a mathematical relationship, has led to the development of techniques such as neural networks. The neural network (NN) approach tries to relate the given input and output obtained from the system. A network tries to recognize the pattern by analyzing the data and then utilize these patterns for solving problems. The nonlinear operation during the training of the network generates the output. In neural networks, the pattern recognition is data dependent and is thus not a closed-form solution. In reference to the present study, a typical multi-layer perceptron (MLP) neural network model is shown in Figure 1. The ability to solve real-world problems, e.g., problems in pattern recognition, data processing and nonlinear control, has made neural networks complementary to the conventional approaches (Bishop, 1994). To test the capabilities of the neural networks in order to recognize the patterns of different outputs, Elkordy et al. (1993) trained three backpropagation networks with normalized reduced mode shapes. The mode shapes were obtained from a simplified two-dimensional frame with beam elements and from a detailed finite element model. Barai and Pandey (1995) generated training examples with various combinations of damage in the bottom chord of steel bridges and identified the reduced stiffness in terms of cross-sectional area. Zhao et al. (1998) concluded that natural frequencies or slope arrays sometimes provide better results than mode shapes and state arrays and that the prediction of one-element damage states is more accurate than the multiple damage states. Slope arrays describe the slopes between two adjacent points in a mode shape and state arrays give the differences in the nodal values between two mode shapes. Hou et al. (2000) showed that the occurrence of damage and the moment when this damage occurs can be clearly determined in the details of the wavelet decomposition of the considered vibration data. Sun and Chang (2002) used the wavelet packet transform based component energies as input to the neural network models for damage assessment. Yun and Bahng (2000) studied the substructuring technique on a two-span truss and a multi-storey frame and found that the elements with large modal strain energy are easily detectable than those with negligible modal strain energy for a particular mode. Marwala (2000) studied the performance of a committee of neural network technique that used frequency response functions, modal properties (i.e., natural frequencies and mode shapes), and wavelet transform data simultaneously in order to identify damage in structures. It was shown that data noise does not influence the performance of the approach. The method proposed in the paper identified damage cases better than the three approaches used individually. The committee approach is known to give results that have a lower mean-

square error (MSE) than the average MSE of the individual methods. Ni et al. (2002) proposed a strategy to locate joint damage and to identify the extent of damage in existing buildings by using the modal component as an input for the three-layered neural network configuration with back propagation algorithm. Zapico and Gonzalez (2006) utilized the natural frequencies obtained from a finite element model to train the multi-layer perceptron network for assessing the overall damage at each floor in a composite two-storey frame. Qian and Mita (2007) applied the Parzen window method for structural damage location and a feed-forward back propagation neural network for identifying the degree of damage in a 5-storey shear building. The proposed algorithm uses only a small number of training data. Zapico et al. (2005) and Gonzalez and Zapico (2008) worked on two different approaches for seismic damage identification in buildings with steel moment-frame structures based on artificial neural network and modal variables. The statistical analysis of the results was successful, but it was shown that the predictions are quite sensitive to the data and modal errors. Bakhary et al. (2010) presented an approach to detect small structural damage in a three-storey frame by using the artificial neural network (ANN) method with progressive substructure zooming. They used the substructure technique together with a multi-stage ANN model to detect the location and extent of the damage. The modal parameters, i.e., frequencies and mode shapes, are used as inputs to ANN. Lautour and Omenzetter (2010) used an auto-regressive (AR) model to fit the acceleration time histories. The coefficients of the AR model were the input and the damage cases or remaining structural stiffness were the output to an ANN. It was concluded that the combinations of AR models and ANNs perform well even on using a small number of damage-sensitive features and limited sensors. Reda Taha (2010) described a damage detection method based on ANN to compute the wavelet energy of acceleration signals acquired from the structures.

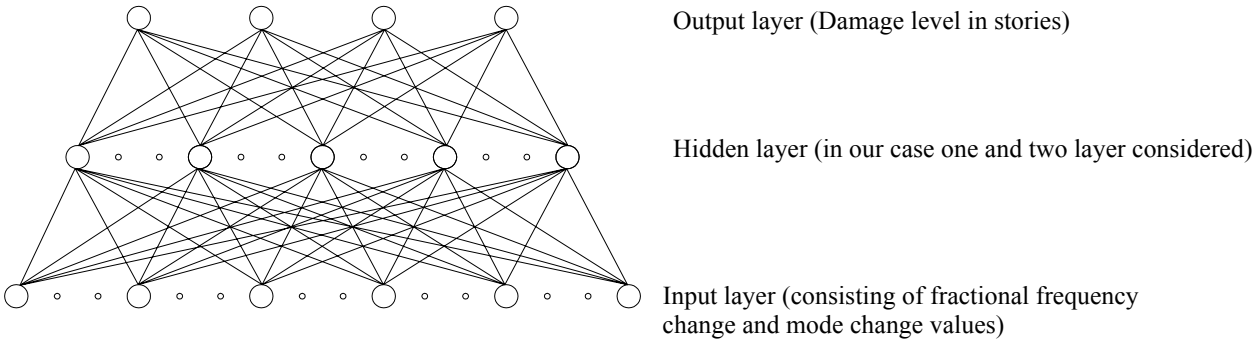

Fig. 1 Typical MLP neural network model with reference to present study

DAMAGE QUANTIFICATION USING MODAL PARAMETERS

The extent of retrofitting at the determined damage location is always of concern. The stability of the structure and approximate cost of repair depend on the quantification of damage in the structure. Many researchers have used frequencies and mode shapes of the structures to indicate the probable existence of damage (Salawu, 1997; Yuen, 1985). In order to determine the level of damage in different storeys of a reinforced concrete building, an approach using neural network is worked out in which changes in the modal parameters of the building as input and respective damages as output are fed to the network for training. This method would be equally applicable to steel structures as well, with the limitation that only those steel members which have been subjected to the ultimate stress, leading to the reduction in story stiffness, can be considered. The nonlinear behaviour of steel is normally idealized as a bilinear relationship, with no stress carrying capacity in the structural members after yielding. Hence, after a steel member has yielded, its stiffness is considered to be zero; however, once it is unloaded, the elastic behaviour is retained, although the stiffness may or may not be same as that in the undamaged structure. Thus, the limitation of this study is that it would be able to determine only the reduction in the storey stiffness of the building and would not be able to determine the reduction in the member stiffness.

The modal parameters of a structure depend on the physical characteristics of the structural members, which are in turn sensitive to the environmental conditions; the environmental conditions are thus bound to affect the modal parameters. However, in the present case, since fractional frequency change is considered for neural network training, variation in frequency in no case would be greater than 0.1 under the assumption that maximum variation in frequency between sunny days and cold weather is not more

than 10%. The fractional frequency change in the case of the same environmental conditions after earthquake damage will be $\left(F_{DA}-F_U\right)/F_U$. On the contrary, in the case of the frequency of the structure determined in non-similar environmental conditions, the fractional frequency change would be $\left[\left(F_{DA}\pm\Delta F_{DA}\right)-F_U\right]/F_U$ or $\left(F_{DA}-F_U\right)/F_U\pm\Delta F_{DA}/F_U$ or $\left(F_{DA}-F_U\right)/F_U\pm 0.1*F_U/F_U$ or $\left(F_{DA}-F_U\right)/F_U\pm 0.1$. Here, F_U denotes the frequency of the undamaged structure in the particular environmental conditions, F_{DA} denotes the actual frequency of the damaged structure in the same environment conditions in which the frequency of the undamaged structure is determined, and ΔF_{DA} denotes the variation due to the environmental factor in the extracted frequency of the damaged structure. For the purpose of calculations, the variation in frequency due to the environmental factor is considered as 10% of the frequency of the undamaged structure, which would be highly conservative in respect of the scenarios where the temperature variations are not extremely high. Further, this assumption is made because the actual frequency of the damaged structure cannot be extracted.

In the above calculations, variation in frequency will not be constant for different environmental conditions, but the maximum relative error in frequency variation can be considered as 0.1 for the extreme case. Further, since the mode shape used for neural network training is normalized to the top of the building, the environmental factor should not be of any concern. The variations in the errors of the estimated damage at various floor levels due to a change in the environmental conditions can be studied, but such a study is beyond the scope of the present work. Further, the acceleration records determined from the recorded ambient vibrations might be contaminated by noise. However, this contamination will not affect the results since the neural network training is carried out by using frequency-domain parameters, not time-domain parameters. Although frequency extraction from a frequency response spectrum is subjected to the judgment of the users, with the help of the mode shape associated with the extracted frequency, the possibility of any misinterpretation can be reduced. In addition, since modal parameters are used to train the network to determine the relative state of floor, the accuracy of experimental results would not matter. The accuracy would be of interest, in case the severity of damage is directly related to the exact quantity of retrofitting to be carried out.

In the present study, the neural network training is based on the unidirectional extraction of modal parameters and not on the bidirectional acquisition of records. The objective is to determine relative damage with a minimum extraction of modal parameters. A limitation of the present study is that only the unidirectional extracted mode shape of the damaged building can be considered for damage quantification. When the mode shape of the considered direction becomes torsional mode shape or the vibration starts in the other direction after damage, that particular mode cannot be extracted. In such a case the study may not be able to produce effective results due to the insufficient input data. The accuracy of the severity of damage for the same level would change, in case bidirectional modal parameters are considered for the unsymmetrical building. Therefore, the accuracy of the equivalent 2D model for neural network based storey level damage severity is studied. The capabilities of trained networks are checked to detect the locations of damage. Two case studies on the analytical models of four- and eight-storey buildings, which are common in India, are presented here. These case studies are not verified with any experimental results, as the study focuses on the comparison of the damage levels to be considered for the neural network training for the most probable floor damage severity.

In this study neural networks are trained by using the MLP of the programme NeuroSolutions (NeuroDimension, 2006). The cross-validation data set considered during the training of the network is 10% of the input data in size. The convergence criterion used for terminating the training of the data is the increase in cross-validation values. Various parameters assumed for the training of networks are given in Table 1.

Table 1: Parameters for Neural Network with Two Hidden Layers

Description	Hidden Layer 1	Hidden Layer 2	Output Layer
Transfer Function	Tanhaxon	Tanhaxon	Sigmoid
Learning Rule	Momentum	Momentum	Momentum
Step Size	1.0	0.1	0.01
Momentum	0.7	0.7	0.7

FOUR-STOREY BUILDING

In the first case study a two bay by two bay four-storey building is considered. The modeling of the building is carried out in SAP 2000 (CSI, 2002) as shown in Figure 2, depicting vertical columns, horizontal beams, and infills as equivalent struts in the form of line sketch. Appropriate dead and live loads along with the wall thicknesses are considered for the modal analysis of the structure. The contributing area of the load shared by each node is used to determine the lumped mass at each storey. The floor stiffness is calculated from the deflection obtained by applying unit load at the upper floor of the storey. The stiffness and mass values of each storey of the undamaged shear frame building are given in Table 2. The derived storey stiffnesses and masses are the characteristics of the equivalent stick model consisting of link elements and lumped masses at the designated storeys of the structure. The stiffness value assigned to a link element represents the combined stiffness of all the respective columns in that storey and the lumped mass value represents the total mass of that particular storey. The modal parameters, i.e., the frequencies and mode shapes of this 2D model, are used for the neural network training. The variations in the lateral stiffnesses of the elements represent the different levels of damage in the different floors of the building. The variations in the stiffnesses of different link elements generate different structural models and accordingly different frequencies and mode shapes of the buildings are obtained. The damage values are considered as the combinations of 0%, 35% and 75% for three damage levels, 0%, 25%, 50% and 75% for four damage levels, and of 0%, 20%, 40%, 60% and 75% for five damage levels. The various damage levels that are considered correspond to light damage, moderate damage, severe damage and extremely severe damage. The damage as high as 75% is easily visible by the naked eye, yet the quantification through visual inspection about the severity of damage in a particular floor would always be questionable, as this involves human judgment at various locations of the damage. Further, a prediction of 75% damage by the neural network suggests replacement of the damaged elements; hence, damage of more than 75% would be an irrelevant damage level for the present study. Also, consideration of only the lower level damage would make the neural network unstable for the determination of a higher level damage severity. The different possible damage combinations are governed by $N_{dc} = N_{dv}^{Ns}$, where N_{dc} is the total number of cases or damage combinations, N_{dv} is the number of damage values, and Ns is the number of storeys in the structure. Thus, for a four-storied building, three damage levels give 81 combinations, four damage levels give 256 combinations, and five damage levels give 625 combinations. The damage combination levels related to various states of the damaged building cases required for the neural network training being large are not mentioned, since it would be difficult to establish the trend of various damage level cases through the changes in frequencies. The stiffness values K, $0.8K$, $0.75K$, $0.65K$, $0.6K$, $0.5K$ and $0.25K$ are assigned to the links for the respective damage values of 0%, 20%, 25%, 35%, 40%, 50%, 60% and 75%, where K denotes the respective storey stiffness of the undamaged structure. A typical set of damage combinations with three damage values is shown in Figure 3. A MATLAB code (MathWorks, 2006) is developed to calculate the following:

a) The fractional frequency change, which is relative change in the natural frequencies of the damaged structure with respect to those of the undamaged structure. For the four-storey building, four values of fractional frequency change for each damage case are calculated.
b) The mode shape change, which is the difference in the mode shapes of the damaged structure with respect to the mode shapes of the undamaged structure. All the mode shapes of the damaged as well as undamaged cases are normalized with respect to the top floor. For the four-storey building, 12 values of mode shape change for each damage case are calculated.
c) The fractional frequency and mode shape changes are considered as input to the neural network and the corresponding storey damage levels for each floor as the output.

1. Three, Four and Five Damage Levels Based Networks

1.1 Network Training

The training of networks with the data containing three, four and five damage level values are carried out by using three randomly shuffled data sets, i.e., Data Set 1, Data Set 2 and Data Set 3. The selection of the number of neurons in the hidden layer is not based on some thumb rule, but the trials of networks are carried out with a single hidden layer and with two hidden layers with the nodes ranging from 4 to 32 in numbers. The selection of the best network, which should be used for training, is determined from the

criterion of minimum mean-square error (MSE) obtained after few seconds of training. The networks selected for the training of three damage levels are (i) 16-16-4, 16-16-4, 16-4-4, (ii) 16-16-4, 16-16-4, 16-16-16-4 in the case of four damage levels, and (iii) 16-16-4, 16-16-4, 16-16-4 in the case of five damage levels, for Data Set 1, Data Set 2 and Data Set 3, respectively. All the data sets are trained upto 40,000 epochs. After the training, the network of 16-16-4 of Data Set 2 is found to give best results for three damage levels. Similarly, the network of 16-16-4 of Data Set 2 and the network of 16-16-4 of Data Set 3 for four damage levels and five damage levels, respectively, give best results. These networks are subsequently used for all studies.

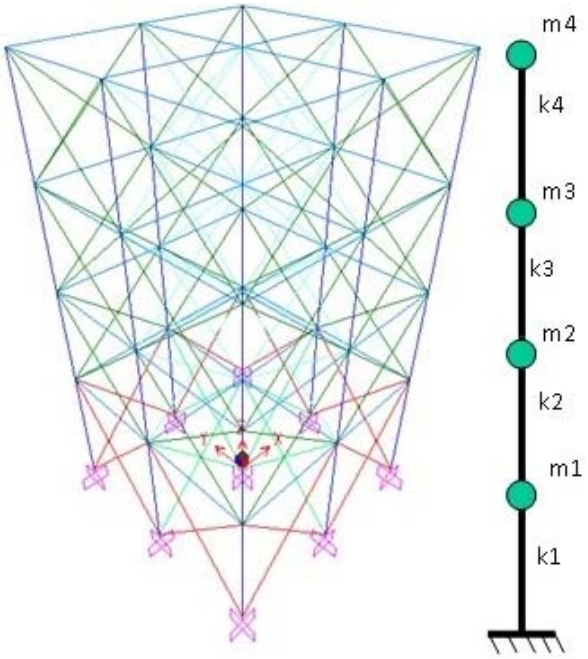

(a) (b)

Fig. 2 Four-storey building: (a) study model, (b) equivalent stick model

Table 2: Stiffness and Mass Details of Four-Storey Building

Storey	Stiffness (kN/m)	Mass (kg)
First	323×10^3	89×10^3
Second	450×10^3	86×10^3
Third	450×10^3	86×10^3
Fourth	443×10^3	64×10^3

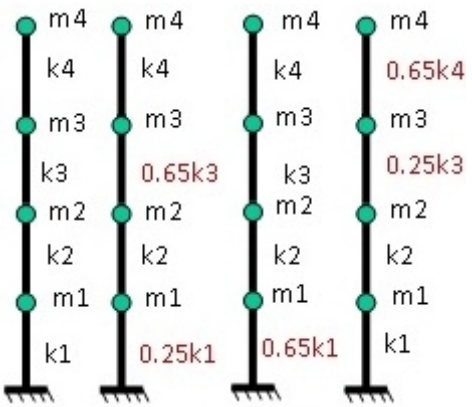

Fig. 3 Typical set of damage combinations for training neural network

1.2 Testing of Network

The testing of the above-selected trained networks is carried out by using randomly selected damage values (RSDV). A total of 81 test samples as detailed below are used for testing; although the test-set data points are small, the test sets are kept same for the comparison of different combinations of damage levels considered for training. The test data sets that are taken contain at least that number of values that are used for training the network:

- the first sample is the undamaged state of the structure;
- 20 samples of the combination of RSDV-1 in the 1st storey and no damage in the 2nd to 4th storeys as in Figure 4(a);
- 20 samples of the combination of RSDV-2 in the 1st storey, RSDV-1 in the 2nd storey and no damage in the 3rd and 4th storeys as in Figure 4(b);
- 20 samples of the combination of RSDV-3 in the 1st storey, RSDV-2 in the 2nd storey, RSDV-1 in the 3rd storey and no damage in the 4th storey as in Figure 4(c); and
- 20 samples of the combination of RSDV-4 in the 1st storey, RSDV-3 in the 2nd storey, RSDV-2 in the 3rd storey and RSDV-1 in the 4th storey as in Figure 4(d);

where RSDV-1, RSDV-2, RSDV-3 and RSDV-4 represent randomly selected damage values between 0–20%, 21–40%, 41–60% and 61–80%, respectively.

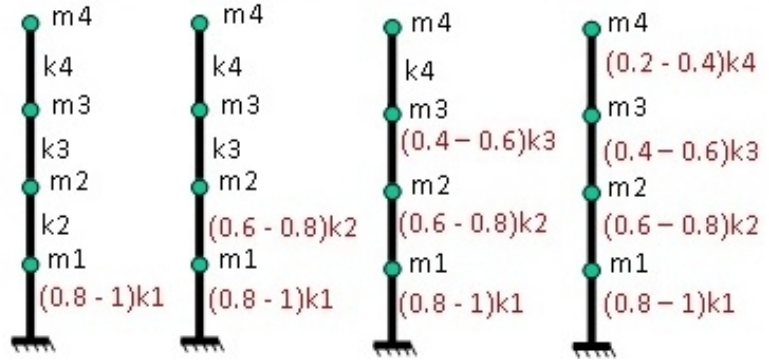

(a) (b) (c) (d)

Fig. 4 Test set of 81 samples (1 undamaged + 20 damaged samples each for 4 storeys) for testing of trained neural networks with damage in (a) one storey, (b) two storeys, (c) three storeys, (d) four storeys

The absolute difference between the predicted percentage and actual percentage of the damage values for each storey is calculated and the maximum difference is considered as the error for that particular case. The median, which reflects the numerical value separating the upper half of a sample from the lower half, the mean, which reflects the central tendency of the sample, and the standard deviation, which measures the variability or diversity from the mean, are determined for the different test damage cases to determine the variation from the expected value. The objective of considering the median is to remove the effect of any wild result obtained for the testing of the neural networks. The median, mean and standard deviation of the error for only the first-storey damage (i.e., D1), first- and second-storey damage (i.e., D1-2), first-, second- and third-storey damage (i.e., D1-3) and all-storey damage (i.e., D1-4) are tabulated in Table 3.

2. Comparison of Three, Four and Five Damage Levels Based Networks

The accuracy of the results obtained from the trained networks is grouped into accurate, substantially accurate, moderately accurate and incorrect:

- results with a maximum difference (among any of the four storeys) of ±3% and less are grouped as accurate,
- results with a maximum difference of ±3–6% are grouped as substantially accurate,
- results with a maximum difference of ±7–9% are moderately accurate, and
- results with a maximum difference more than ±9% are called incorrect.

Table 3: Errors from Trained Networks for Four-Storey Building

Damage Combination		D1	D1-2	D1-3	D1-4
Three Damage Levels	Median	6	9	12	9
	Mean	5.9	7.8	11.2	8.5
	Standard Deviation	3.5	2.3	1.5	0.9
Four Damage Levels	Median	1	3	2	3
	Mean	1.4	3	2	2.8
	Standard Deviation	1	1	1	1
Five Damage Levels	Median	1	1	1	1
	Mean	1	1.7	1.2	1.3
	Standard Deviation	0	0.8	0.5	0.7

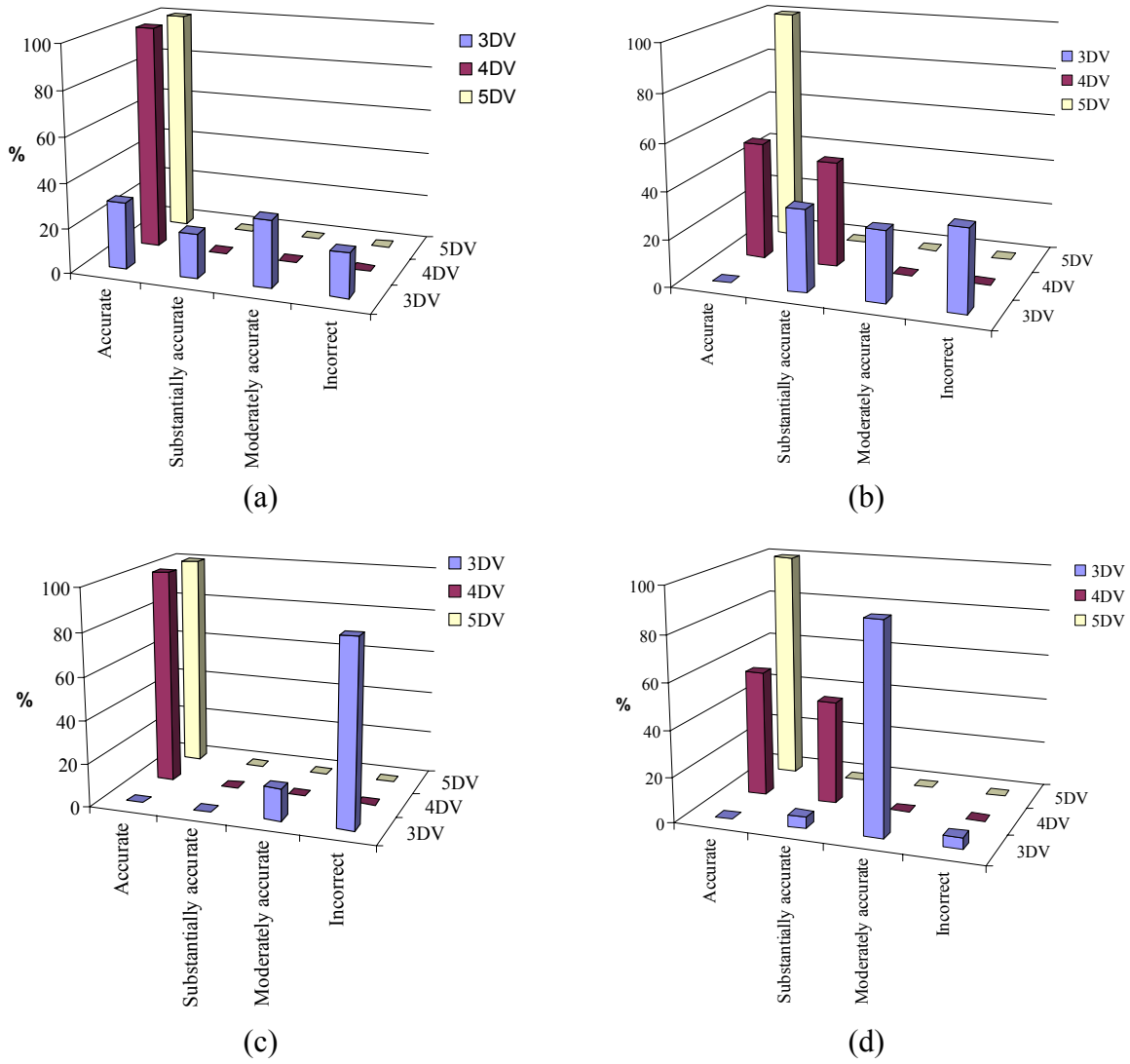

Fig. 5 Efficiencies of three, four and five damage level based networks for randomly damaged (a) only first storey, (b) first and second storeys, (c) first, second and third storeys and (d) all storeys, in four-storey building

The efficiencies of the results obtained from the networks trained with three, four and five damage levels are plotted in Figure 5. The network trained with the data set of the combinations of three damage

values is found to give several incorrect results during the testing. The network trained with the data set of the combinations of four damage values gives either accurate or substantially accurate values. The network trained with the data set of the combinations of five damage values gives all accurate values even in the case of all-storey damage. The accuracy of the output obtained is dependent on the extent of damage, i.e., the number of storeys in which the damage has occurred. A higher number of damaged storeys gives less accurate results. The results obtained from the networks trained with the data sets consisting of fractional frequency changes, mode shape changes and five levels of damage are accurate enough to be relied upon for the location and severity of damage in the four-storey structure.

EIGHT-STOREY BUILDING

In the second case study a four bay by four bay eight-storey building is considered. The model is generated in SAP 2000 (CSI, 2002) as shown in Figure 6. As in the case of four-storey building, an equivalent stick model is generated. The derived stiffness and mass values of each storey for the stick model are tabulated in Table 4.

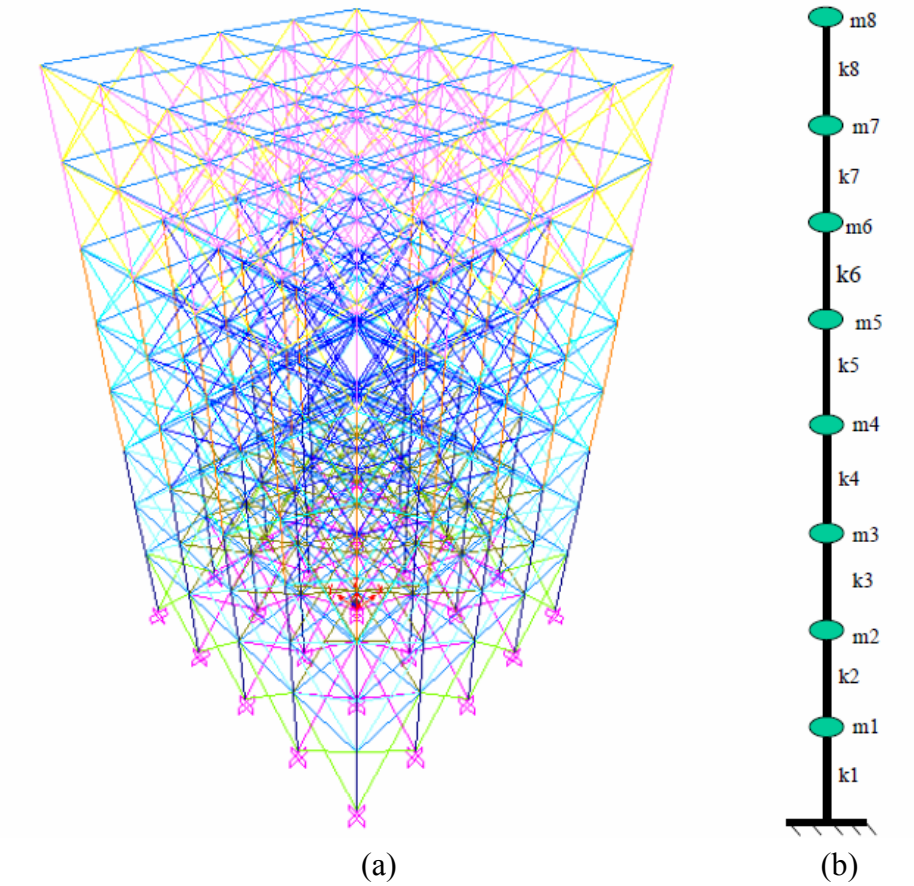

Fig. 6 Eight-storey building: (a) study model, (b) equivalent stick model

Table 4: Stiffness and Mass Details of Eight-Storey Building

Storey	Stiffness (kN/m)	Mass (kg)
First	1256×10^3	3659×10^2
Second	1838×10^3	3501×10^2
Third	1811×10^3	3394×10^2
Fourth	1623×10^3	3288×10^2
Fifth	1623×10^3	3288×10^2
Sixth	1607×10^3	3193×10^2
Seventh	1445×10^3	3098×10^2
Eighth	1412×10^3	2477×10^2

1. Three and Four Damage Levels Based Network

1.1 Network Training

The case study to quantify damage in the eight-storey building is checked on three and four damage level based networks. The training samples for both three damage level and four damage level based networks are considered as same to appreciate the difference in the efficiencies of both the networks. In the case of three damage level based network, the training data set consists of $3^8 = 6{,}561$ samples, whereas in the case of four damage levels a total of $4^8 = 65{,}536$ combinations are possible. These combinations are randomized and a reduced data set of 6553 samples, which are approximately 10% of the total number of combinations, is considered for training. The effect of variations in the samples to be considered for neural network training is beyond the scope of the present study. A MATLAB code (MathWorks, 2006) is developed to find the fractional frequency changes and mode shape changes as in the case of four-storey building. This provides 64 inputs to the neural network with eight outputs (i.e., the damage in various floors). The data sets are checked for the best network as explained in the previous section. The network 64-48-48-8 in the case of three damage levels and the network 64-64-64-8 for four damage levels are selected for testing.

1.2 Testing of Network

The test set consists of 81 test samples, which comprise first sample as the sample in the undamaged state and further 10 samples with the following combinations:

- RSDV-a in the 1st storey and no damage in the 2nd to 8th storeys;
- RSDV-b in the 1st storey, RSDV-a in the 2nd storey and no damage in the 3rd to 8th storeys;
- RSDV-c in the 1st storey, RSDV-b in the 2nd storey, RSDV-c in the 3rd storey and no damage in the 4th to 8th storeys;
- RSDV-d in the 1st storey, RSDV-c in the 2nd storey, RSDV-b in the 3rd storey, RSDV-a in the 4th storey and no damage in the 5th to 8th storeys;
- RSDV-e in the 1st storey, RSDV-d in the 2nd storey, RSDV-c in the 3rd storey, RSDV-b in the 4th storey, RSDV-a in the 5th storey and no damage in the 6th to 8th storeys;
- RSDV-f in the 1st storey, RSDV-e in the 2nd storey, RSDV-d in the 3rd storey, RSDV-c in the 4th storey, RSDV-b in the 5th storey, RSDV-a in the 6th storey and no damage in the 7th and 8th storeys;
- RSDV-g in the 1st storey, RSDV-f in the 2nd storey, RSDV-e in the 3rd storey, RSDV-d in the 4th storey, RSDV-c in the 5th storey, RSDV-b in the 6th storey, RSDV-a in the 7th storey and no damage in the 8th storey; and
- RSDV-h in the 1st storey, RSDV-g in the 2nd storey, RSDV-f in the 3rd storey, RSDV-e in the 4th storey, RSDV-d in the 5th storey, RSDV-c in the 6th storey, RSDV-b in the 7th storey and RSDV-a in the 8th storey;

where RSDV-a, RSDV-b, RSDV-c, RSDV-d, RSDV-e, RSDV-f, RSDV-g and RSDV-h represent randomly selected damage values between 0–10%, 11–20%, 21–30%, 31–40%, 41–50%, 51–60%, 61–70% and 71–80%, respectively.

As for the four-storey building, difference between the expected and output damage values for each storey is calculated and the maximum of the differences over all the storeys is extracted as the error. The median, mean and standard deviation of errors are given in Table 5.

2. Comparison of Three and Four Damage Levels Based Networks

The results are grouped into different categories of accuracy as explained in the previous section. The efficiencies of different trained networks are shown in Figures 7 and 8. It is seen from these figures that the networks trained with the data set of the combinations of three damage values give some incorrect results, while the networks trained with the data set of the combinations of four damage values give accurate and substantially accurate values on considering the worst case of "all storeys" damage. Thus, the results obtained from the networks trained with the data set consisting of the fractional frequency changes, mode shape changes and four levels of damage are accurate enough to be relied upon for the location and severity of damage in the eight-storey structure.

Table 5: Errors from Networks for Eight-Storey Building

Tested Damage Combination	Random Values	a	b	c	d	e	f	g	h
Three Damage Levels	Median	3	6	7	7	6	8	9	9
	Mean	3	5.4	6.7	6.6	6.4	8.1	8.9	8.7
	Standard Deviation	0	0.7	0.5	0.7	0.5	0.3	0.7	1.1
Four Damage Levels	Median	5	5	4	4	3	4	4	3
	Mean	5.1	5	4	4	3.4	3.8	3.9	2.7
	Standard Deviation	0.3	0	0	0	0.5	0.4	0.3	0.5

Here, a, b, c, d, e, f, g and h represent the damage in the "1st storey only", "1st and 2nd storeys", "1st, 2nd and 3rd storeys", "1st, 2nd, 3rd and 4th storeys", "1st, 2nd, 3rd, 4th and 5th storeys", "1st, 2nd, 3rd, 4th, 5th and 6th storeys", "1st, 2nd, 3rd, 4th, 5th, 6th and 7th storeys" and "all storeys" cases, respectively.

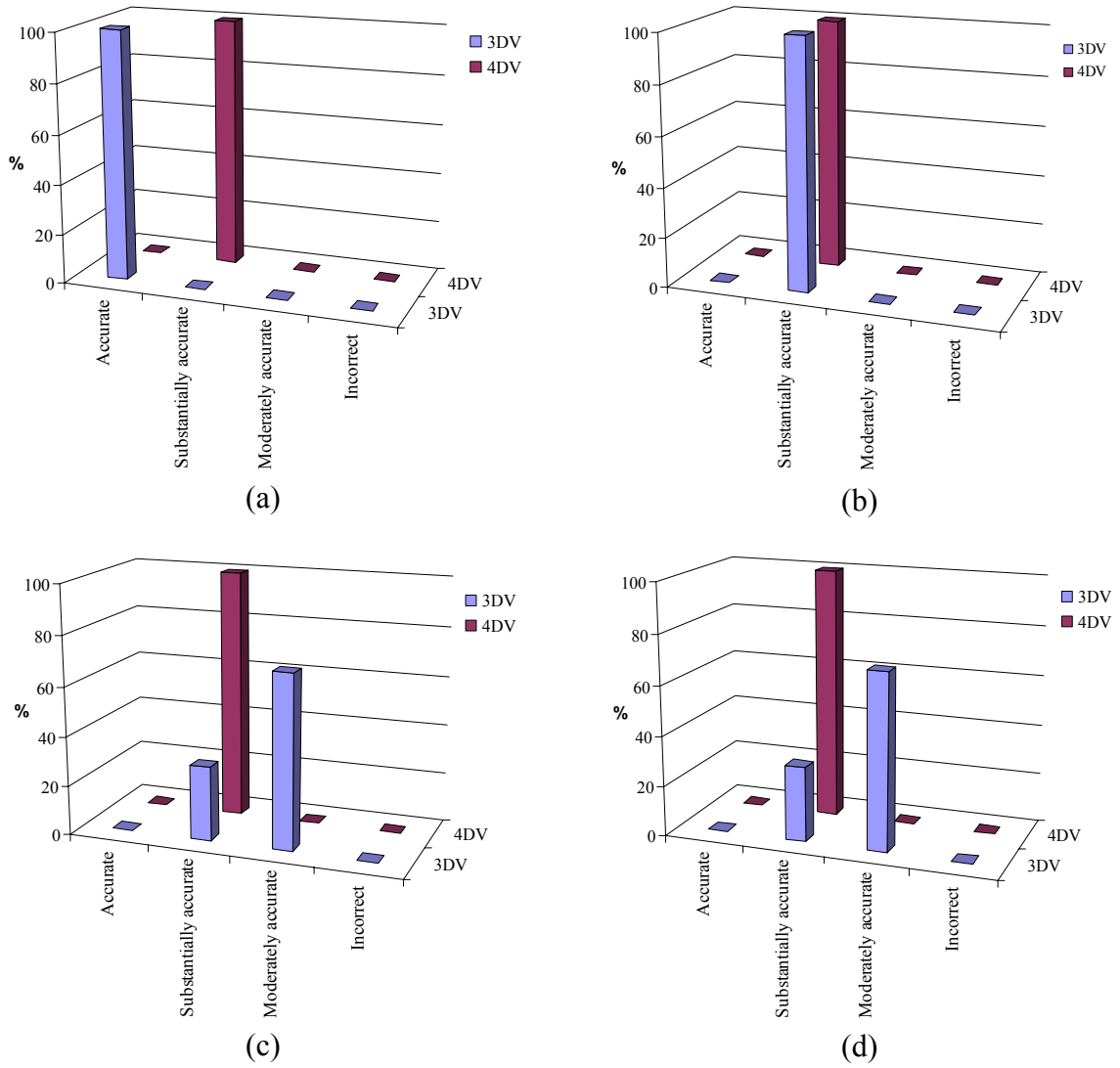

Fig. 7 Efficiencies of three and four damage level based networks for randomly damaged (a) only first storey, (b) first and second storeys, (c) first to third storeys and (d) first to fourth storeys, in eight-storey building

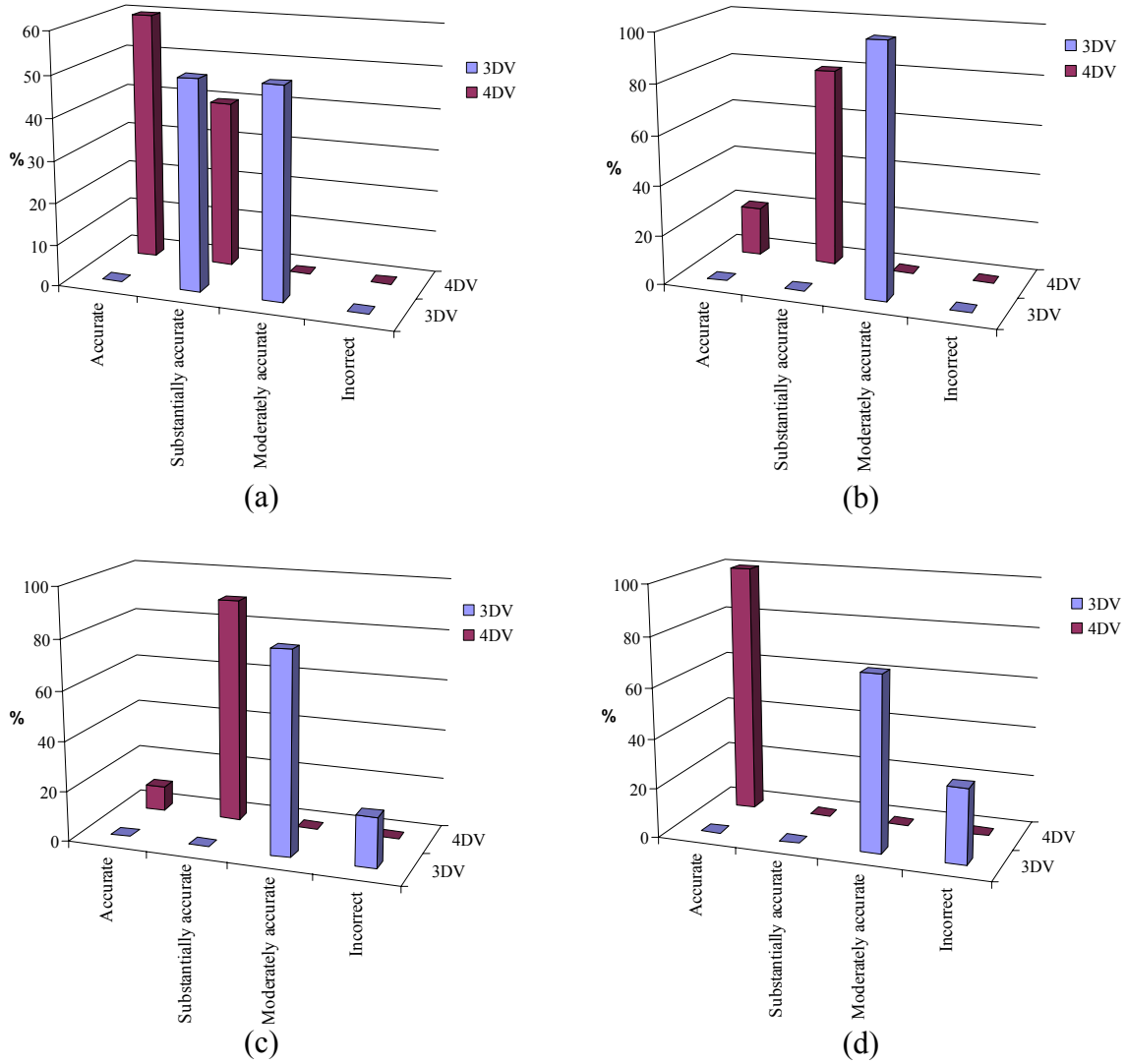

Fig. 8 Efficiencies of three and four damage level based networks for randomly damaged (a) first to fifth storeys, (b) first to sixth storeys, (c) first to seventh storeys and (d) first to eight storeys, in eight-storey building

DISCUSSION OF RESULTS

The results of study are discussed with reference to the two models considered, i.e., four- and eight-storey buildings.

1. Four-Storey Building

The number of training samples generated with the combinations of three damage values is not sufficient for the procedure followed to quantify the damage, as the accuracy of the results is not found to be satisfactory. The number of training samples generated with the combinations of four damage values is quite satisfactory, but the best results are achieved with the combinations of five damage values. The standard deviations show that variations in the results decrease with an increase in the number of damage levels considered for the training of the data.

2. Eight-Storey Building

Although the number of training samples used for training the network with the combinations of three damage values is quite large, the data set lacks sufficient information for the neural network to generate the pattern and quantify the damage successfully. The number of training samples generated with the combinations of four damage values is huge, hence a reduced number, approximately same as that for the case of three damage values, is taken and the results are observed to be satisfactory. The middle storey of the eight-storey building is found to be more unpredictable for quantifying the damage than with respect

to the lower and higher storeys of the building. The damage quantified for the four-storey building with four damage value combinations is more accurate than the damage quantified for the eight-storey building with four damage value combinations and more than 25 times the samples used for the four-storey building.

To summarize the method for the real-world applications, following steps are to be followed for identifying the damaged storeys and for quantifying damage in various storeys:

1. Ambient vibration testing should be done to determine the frequencies and mode shapes of the undamaged building.
2. The mathematical model of the building should be generated and updated in any standard structural analysis program, such that the frequencies of the building match the experimental frequencies.
3. The sets of frequencies and mode shapes should be determined for various damage combinations of different storeys from the analytical model. These damage combinations represent a set of damage states, whereas a set of damage sets implies damage in different storeys.
4. The ratio of difference between the undamaged and damaged states to the undamaged state is used as one part of the input for neural network training as far as the frequency parameter is concerned.
5. The differences in the mode shapes of the damaged state with respect to the undamaged state, with the top node normalized to unity, form another part which is also used as input for the neural network as far as the mode shape parameter s concerned.
6. This combination of the relative frequency change ratio and change in mode shape is finally used for training the neural network.
7. The trained network should be used to determine the damage, once an earthquake occurs.
8. The ambient vibration testing of the building should be done again after the occurrence of the earthquake and the frequencies and mode shapes of the structure should be determined.
9. The so-obtained frequencies and mode shapes should be given as input to the neural network to locate the damage and to determine the extent of damage.

CONCLUSIONS AND FUTURE RESEARCH

The combination of frequency change and mode shape change can be used to locate and quantify damage in an important building in the event of an earthquake. The database of the modal parameters of various important buildings can be maintained as signatures of those buildings in records. This database can be used to determine the extent of deterioration in such buildings in the event of an earthquake.

It is evident from the comparison of different damage level combinations considered that the number of training samples used for training a network should be sufficient and the data set should contain sufficient information so that the neural network can generate a correct pattern from the data set. Thus, the information about a particular building can be increased by considering a 3D model of the building, instead of the 2D model considered in the present study.

The probability of predicting accurate damage in a building decreases with an increase in the number of damaged storeys. Hence, damage prediction in different storeys of the building should be complemented with the other methods of damage prediction.

This study has focused only on the stiffness reduction of the storeys of the building. Future work can be directed towards predicting stiffness reduction of various members in the buildings.

REFERENCES

1. Bakhary, N., Hao, H. and Deeks, A.J. (2010). “Structure Damage Detection Using Neural Network with Multi-stage Substructuring”, Advances in Structural Engineering, Vol. 13, No. 1, pp. 95–110.
2. Barai, S.V. and Pandey, P.C. (1995). “Vibration Signature Analysis Using Artificial Neural Networks”, Journal of Computing in Civil Engineering, ASCE, Vol. 9, No. 4, pp. 259–265.
3. Bishop, C.M. (1994). “Neural Networks and Their Applications”, Review of Scientific Instruments, Vol. 65, No. 6, pp. 1803–1832.
4. CSI (2002). “SAP2000: Integrated Software for Structural Analysis and Design—Analysis Reference Manual, Version 8.0”, Computers and Structures, Inc., Berkeley, U.S.A.

5. Elkordy, M.F., Chang, K.C. and Lee, G.C. (1993). "Neural Networks Trained by Analytically Simulated Damage States", Journal of Computing in Civil Engineering, ASCE, Vol. 7, No. 2, pp. 130–145.
6. Gonzalez, M.P. and Zapico, J.L. (2008). "Seismic Damage Identification in Buildings Using Neural Networks and Modal Data", Computers & Structures, Vol. 86, No. 3-5, pp. 416–426.
7. Hou, Z., Noori, M. and Amand, R.S. (2000). "Wavelet-Based Approach for Structural Damage Detection", Journal of Engineering Mechanics, ASCE, Vol. 126, No. 7, pp. 677–683.
8. Lautour, O.R.D. and Omenzetter, P. (2010). "Damage Classification and Estimation in Experimental Structures Using Time Series Analysis and Pattern Recognition", Mechanical Systems and Signal Processing, Vol. 24, No. 5, pp. 1556–1569.
9. Marwala, T. (2000). "Damage Identification Using Committee of Neural Networks", Journal of Engineering Mechanics, ASCE, Vol. 126, No. 1, pp. 43–50.
10. MathWorks (2006). "MATLAB® 7: Getting Started Guide, Version 7.2", The MathWorks, Inc., Natick, U.S.A.
11. NeuroDimension (2006). "NeuroSolutions: User's Manual, Version 5.04", NeuroDimension, Inc., Gainesville, U.S.A.
12. Ni, Y.Q., Wang, B.S. and Ko, J.M. (2002). "Constructing Input Vectors to Neural Networks for Structural Damage Identification", Smart Materials and Structures, Vol. 11, No. 6, pp. 825–833.
13. Qian, Y. and Mita, A. (2007). "Structural Damage Identification Using Parzen-Window Approach and Neural Networks", Structural Control and Health Monitoring, Vol. 14, No. 4, pp. 576–590.
14. Reda Taha, M.M. (2010). "A Neural-Wavelet Technique for Damage Identification in the ASCE Benchmark Structure Using Phase II Experimental Data", Advances in Civil Engineering, Vol. 2010, Paper 675927.
15. Salawu, O.S. (1997). "Detection of Structural Damage through Changes in Frequency: A Review", Engineering Structures, Vol. 19, No. 9, pp. 718–723.
16. Sun, Z. and Chang, C.C. (2002). "Structural Damage Assessment Based on Wavelet Packet Transform", Journal of Structural Engineering, ASCE, Vol. 128, No. 10, pp. 1354–1361.
17. Yuen, M.M.F. (1985). "A Numerical Study of the Eigen Parameters of a Damaged Cantilever", Journal of Sound and Vibration, Vol. 103, No. 3, pp. 301–310.
18. Yun, C.B. and Bahng, E.Y. (2000). "Substructural Identification Using Neural Networks", Computers & Structures, Vol. 77, No. 1, pp. 41–52.
19. Zapico, J.L. and Gonzalez, M.P. (2006). "Numerical Simulation of a Method for Seismic Damage Identification in Buildings", Engineering Structures, Vol. 28, No. 2, pp. 255–263.
20. Zapico, J.L., Gonzalez, M.P. and Worden, K. (2003). "Damage Assessment Using Neural Networks", Mechanical Systems and Signal Processing, Vol. 17, No. 1, pp. 119–125.
21. Zhao, J., Ivan, J.N. and DeWolf, J.T. (1998). "Structural Damage Detection Using Artificial Neural Networks", Journal of Infrastructure Systems, ASCE, Vol. 4, No. 3, pp. 93–101.

ISET Journal of Earthquake Technology, Paper No. 520, Vol. 49, No. 1-2, March-June 2012, pp. 37–52

EFFECT OF SEISMIC OBLIQUE WAVES ON DYNAMIC RESPONSE OF AN EMBEDDED FOUNDATION

Salah Messioud*, Badreddine Sbartai** and Daniel Dias***

*Department of Civil Engineering, University of Jijel, 18000 Jijel, Algeria
**Department of Civil Engineering, University of Skikda, 21000 Skikda, Algeria
***Department of Geotechnical and Civil Engineering, Polytech Grenoble, 38400 Saint-Martin-d'Hères, France

ABSTRACT

This study analyzes the influence of soil-structure interaction on the seismic response of a three-dimensional (3-D) rigid foundation on the surface of a viscoelastic soil limited by bedrock. The vibrations are assumed to result only from the P, SV, SH and R harmonic seismic waves. The key step here is the characterization of the soil-foundation interaction with the impedance matrix on one hand and input motion matrix on the other hand. The mathematical approach is based on the method of integral equations in the frequency domain using the formalism of Green's functions for a layered soil. This approach is applied to analyze the effect of soil-structure interaction on the seismic response of the foundation as a function of the kind of incident wave, angle of wave incidence, wave frequency and embedment of foundation.

KEYWORDS: Wave Propagation, BEM-TLM Method, Soil-Structure Interaction

INTRODUCTION

The analysis of the behavior of foundations under dynamic loads has grown considerably over the past four decades. Stringent security requirements imposed on the design of certain types of structures have played an important role in the development of analytical methods. The key step in studying the dynamic response of foundations is the determination of the relationship between various forces. This relationship, which results in displacements, is expressed by using impedance functions (i.e., dynamic stiffnesses) or compliance functions (i.e., dynamic flexibilities). The consideration of the soil-structure interaction in the analysis of the dynamic behaviour of foundations allows us to realistically take into account the influence of soils on their vibrations.

A myriad of methods have been proposed to solve the problem of soil-structure interaction. To simplify the problem, various linear-analysis techniques have been developed. One of the most commonly used approaches is the substructuring method that allows the problem to be analyzed in two parts (Aubry and Clouteau, 1992; Kausel et al., 1978; Pecker, 1984). In this approach the dynamic response of superstructure elements and substructure are examined separately. The analysis of the foundation system can be reduced to the study of dynamic stiffnesses at the soil-foundation interface (known as impedance functions) and driving forces from the incident waves. The kinematic interaction of the foundation with the incident waves is implemented in the form of a driving-force vector.

The determination of foundation response is a wave propagation problem. Due to the mixed-boundary conditions of the problem (i.e., displacement compatibility with the stress distribution underneath the foundation and zero tension outside), the solutions are complex. The determination of impedance functions and forces of movement related to the incident waves is a complex process. Several studies have been conducted on the dynamic response of foundations by using the finite-element and boundary-element methods. Wong and Luco (1978) have shown the importance of the effect of the non-verticality of SV and SH harmonics on the response of a foundation.

Apsel and Luco (1987) used an integral-equation approach based on Green's functions for multilayered soils to calculate the impedance functions of a foundation. Using this approach, Wong and Luco (1986) studied the dynamic interaction between the rigid foundations resting on half-space. Boumekik (1985) studied the problem of 3-D foundations embedded in the soil limited by a rigid substratum. The finite-element method was applied by Kausel et al. (1978), Kausel and Roësset (1981), and Lin and Tassoulas (1986) to determine the behavior of rigid foundations placed on or embedded in a soil layer limited by a rigid substratum. A formulation of the boundary-element method in the frequency

domain has also been developed to address the wave-propagation problems of soil-structure interaction and structure-soil-structure interaction, which limits discretization at the interface of soil and foundation. In this approach, the displacement field is formulated as an integral equation in terms of Green's functions (Beskos, 1987; Aubry and Clouteau, 1992; Qian and Beskos, 1996; Karabalis and Mohammadi, 1998; Mohammadi, 1992). Çelebi et al. (2006) used the boundary-element method with integral formulation (i.e., BIEM) to compute the dynamic impedance of foundations. In this context, the analytical solutions of 3-D wave equations in cylindrical coordinates in a layered medium, while satisfying the necessary boundary conditions, have been employed by Liou (1993) and Liou and Chung (2009). Sbartai and Boumekik (2008) used the BEM-TLM method to calculate the dynamic impedance of rectangular foundations placed or embedded in a layered soil limited by a substratum and also the propagation of vibrations in the vicinity of a vibrating foundation. They further used the BEM-TLM method to analyze the effects of some parameters on the dynamic response of those foundations. These parameters are the depth of the substratum, embedment, masses and shape of the foundation, soil heterogeneity, and frequency. However, Sbartai and Boumekik (2006, 2007) have studied the dynamic response of two square foundations placed or embedded in a layered soil limited by a substratum. Spryakos and Xu (2004) have developed a hybrid BEM-FEM method and have conducted several studies for the parametric analysis of soil-structure interaction.

Recently, McKay (2009) used the reciprocity theorem based on the BIEM to analyze the influence of soil-structure interaction on the seismic response of foundations. Suárez et al. (2002) applied the BIEM to determine the seismic response of an L-shaped foundation. In addition, experimental work has been carried out by researchers in Japan to determine the effect of soil-structure interaction on the response of real structures (Fujimori et al., 1992; Ohtsuka et al., 1996; Mizuhata et al., 1988; Watakabe et al., 1992; Imamura et al., 1992).

In the present study, a solution is derived from the boundary element method (BEM) in the frequency domain with constant quadrilateral elements and the thin-layer method is used to analyze the influence of soil-structure interaction on the response of seismic foundations. The results are presented as the coefficients of movement in the matrix $\left[S^*\right]$ and in terms of displacement as a function of dimensionless frequency, angles of incidence (vertically and horizontally) and embedment of foundation. This paper is in continuation of the work published in Sbartai and Boumekik (2008) where the impedance functions have been well studied in detail. Therefore, those impedance functions are not discussed in this paper.

FOUNDATION RESPONSE TO WAVES OF SEISMIC ORIGIN

1. Physical Model and Basic Equations

The geometry of the calculation model is shown in Figure 1. We consider a 3-D, rigid, massless, surface foundation of an arbitrary shape S in full contact with a homogeneous, isotropic and linearly-elastic soil that is limited by a bedrock. The soil is characterized by its density ρ, shear modulus G, damping coefficient β and Poisson's ratio ν. The foundation is subjected to the harmonic oblique-incident waves that are time-dependent, i.e., P, SV, SH and R.

The movement of an arbitrary point ζ can be obtained by solving the wave equation:

$$\left(C_P^2 - C_S^2\right)u_{,ij} + C_S^2\, u_{,jj} - \omega^2 u_i = 0 \tag{1}$$

where C_S and C_P are the velocities of shear and compression waves respectively and ω the angular frequency of excitation. Further, u_i is the component of the harmonic displacement vector in the x-direction; $u_{,ij}$ is the partial derivative of the displacement field with respect to x and y; and $u_{,jj}$ is the second partial derivative of the displacement field with respect to y. The solution of Equation (1) may be expressed by the following integral equation:

$$u_j\left(x,\omega\right) = \int_S G_{ij}\left(x,\xi,\omega\right) t_i\left(\xi,\omega\right) \mathrm{d}s\left(\xi\right) \tag{2}$$

with G_{ij} denoting Green's functions at the point i due to unit harmonic loads (vertical and horizontal) on the ground at the point j, and t_i being the load (i.e., traction) distributed over an area of the soil.

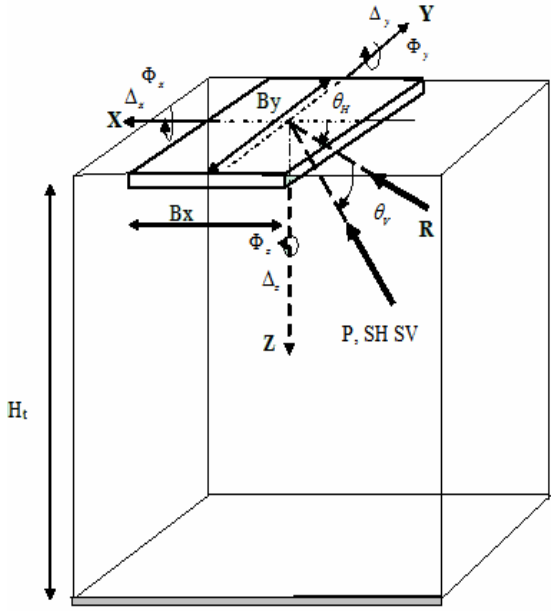

Fig. 1 Geometry of foundation subjected to harmonic seismic waves

The medium is continuous and, therefore, the relationship in Equation (2) is very difficult to solve. However, if the soil mass is discretized appropriately, this relationship can be made algebraic and displacements can be calculated. The key step of this study is to determine the impedance matrix linking the harmonic forces applied with the resulting harmonic displacements. Even with a continuous medium, the determination of the impedance matrix is very difficult, if not impossible, due to the propagation problem and mixed-boundary conditions. However, if the medium is discretized both vertically and horizontally, it is possible to make the problem algebraic by considering the variation of interface displacement to be a linear function. The principle of horizontal and vertical discretizations of the soil mass is shown in Figure 2, where H_t denotes the height of the soil mass, h_1 the height of the sublayer 1, N_x the number of elements in the *x*-direction for a horizontal plane, N_y the number of elements in the *y*-direction for a horizontal plane, N_z the number of soil layers, N the total number of elements in the soil-foundation interface, and B_x and B_y the dimensions of the foundation. The principle of vertical discretization is based on the division of every soil layer into a number of sublayers of height h_j with similar physical characteristics. Each sublayer is assumed to be horizontal, viscoelastic, and isotropic, and is characterized by the Lame constant λ_j, shear modulus μ_i and density ρ_j. The bedrock at the depth H_t is considered infinitely rigid and is not discretized. The reflected wave is assumed to be total and the displacements null.

Within a given sublayer, the displacement is assumed to be a linear function of the interface displacements above and below. This is true when the height of the sublayer is small in relation to the wavelength considered (in the order of $\lambda/10$). This method is comparable to the FEM in the sense that the movements within each sublayer are completely defined from the displacements in the middle of the interfaces. The interaction between the elements is done only through their nodes. The degrees of freedom of the soil mass are thus reduced to the degrees of freedom of the nodes. The stiffness matrix of the soil mass is obtained in a manner similar to how it is determined in the FEM. This technique developed by Lysmer and Waas (1972) is known as the thin-layer method (TLM) and used mainly for horizontal soil layers. This method has the advantage of making the problem algebraic and thus obtains Green's functions by applying the BEM on the soil-foundation interface. For this reason, a horizontal discretization of the soil-foundation interface is established.

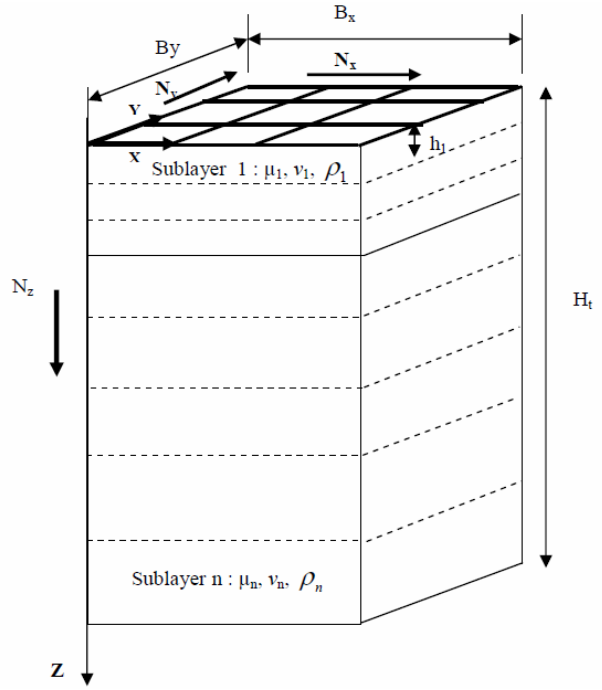

Fig. 2 Model of calculation

The horizontal discretization permits a subdivision of any horizontal soil-foundation interface by the elements of square sections, S_k. The constant-moving average is replaced by the movement of the center in these elements as shown in Figure 2 and it is assumed that stress distribution is uniform in these elements. For the sake of simplicity in integration calculations and economy in computational time, the square elements are approximated as disc elements. If unit loads are applied to the disc j (along the directions x, y, z), Green's functions at the center of the disc i can be determined. By successively applying these loads on all the discs, the flexibility matrix of the soil mass at a given frequency ω can be formed. The discretized model to calculate the impedance functions of the foundation is also presented in Figure 2. In this model, Equation (2) is expressed in an algebraic form as follows:

$$u_j = \sum_{i=1}^{N} \int_S G_{ij} t_i \mathrm{d}s \tag{3}$$

2. Determination of Green's Functions by TLM

Green's functions for a layered stratum are obtained by an inversion of the thin-layer stiffness matrix by using spectral-decomposition procedure by Kausel and Peek (1982). The advantage of the thin-layer-stiffness matrix technique over the classical transfer-matrix technique for finite layers and the finite-layer-stiffness matrix technique (Kausel and Roësset, 1981) is that the transcendental functions in the layered-stiffness matrix are linearized.

In this work, the body B represents a layered stratum resting on a substratum base with n horizontal layer interfaces defined by $z = z_1, z_2, ..., z_n$ and with the layer j defined by $z_n < z < z_{n+1}$, as shown in Figure 3. The medium of the nth layer of thickness h_n is assumed to be homogeneous, isotropic, and linearly elastic. For the body B, Green's functions in frequency domain are obtained with the help of the TLM. According to the thin-layer theory of Lisper and Waas (1972), displacements in each sublayer vary linearly from one plane to another while continuing in the relevant direction x, y or z. Thus, the displacements in each sublayer are obtained by the linear interpolation of nodal displacements at the interface of the sublayer n as follows:

$$U^{(n)}(z) = (1-\eta)U^n + \eta U^{n+1} \tag{4a}$$

$$V^{(n)}(z) = (1-\eta)V^n + \eta V^{n+1} \tag{4b}$$

$$W^{(n)}(z) = (1-\eta)W^n + \eta W^{n+1} \tag{4c}$$

where $\eta = (z - z_n)/h_n$ with $0 \le \eta \le 1$. Further, $U^{(n)}$, $V^{(n)}$ and $W^{(n)}$ are the displacements along the x-, y- and z-axes as the functions of z in the layer j, and U^n, V^n and W^n are their nodal values respectively at the interface layer $z = z_n$. Green's functions are obtained as

$$G_{ij}^{mn} = \sum_{l=1}^{2N} \frac{a_{\alpha\beta}\varphi_i^{ml}\varphi_j^{nl}}{k^2 - k_l^2} \tag{5}$$

with $a_{\alpha\beta} = 1$, if $\alpha = \beta$; $a_{\alpha\beta} = k/k_l$, if $\alpha \neq \beta$; and $i, j = x, y, z$. Further, k and k_l represent the wave numbers, m represents the interface where the load is applied, and n represents the interface where Green's functions are calculated.

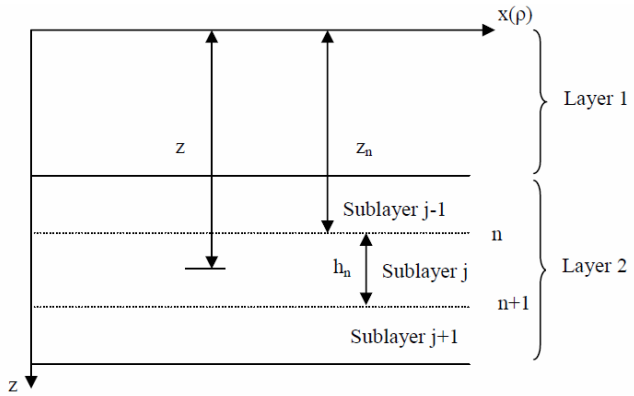

Fig. 3 Geometry of soil layers represented by body *B*

Green's functions so obtained are complex and constitute the starting point for the determination of the flexibility matrix of an arbitrary soil volume. However, on considering the geometry of the foundation, a system of Cartesian coordinates is adopted. The above expressions of U, V, W and Green's functions are in fact the terms of the flexibility matrix of the soil. The determination of this flexibility matrix gives the impedance functions of one or several foundations and the amplitudes of vibrations in the neighborhood of a foundation (Sbartai and Boumekik, 2007, 2008).

The viscoelastic soil behavior is easily introduced in the above formulation by simply replacing the elastic constants λ and G with their complex values,

$$\lambda^*(Z) = \lambda(1 + 2i\beta) \tag{6a}$$

$$\mu^*(Z) = \mu(1 + 2i\beta) \tag{6b}$$

respectively, where β is the hysteretic damping coefficient.

CALCULATION MODEL

The total displacement matrix of the soil is obtained by a successive application of unit loads on the constituents of the discretized solid ground. The displacements in the soil are then expressed as

$$\{u\} = [G]\{t\} \tag{7}$$

where the vectors $\{u\}$ and $\{t\}$ denote the nodal values of the amplitudes of displacements and tractions respectively at the soil-foundation interface, and $[G]$ denotes the flexibility matrix of the soil.

When the foundation is in place, it requires different components of soil displacements consistent with the rigid-body motions. The compatibility of displacements at the contact area S between the soil and the rigid foundation leads to the matrix equation,

$$\{u\} = [R]\{\Delta\} \tag{8}$$

where

$$[R] = \begin{bmatrix} 1 & 0 & 0 & 0 & z & y \\ 0 & 0 & 0 & -z & 0 & x \\ 0 & 0 & 1 & y & -x & 0 \end{bmatrix} \tag{9}$$

denotes the transformation matrix; $\{\Delta\} = \{\Delta_x \quad \Delta_y \quad \Delta_z \quad \Phi_x \quad \Phi_y \quad \Phi_z\}^T$ denotes the displacement vector; and $\Delta_i \ (i = x, y, z)$ represents the translations and $\Phi_i \ (i = x, y, z)$ the rotations (see Figure 1).

If $\{P\}$ denotes the vector of loads applied to the foundation, the equilibrium between the loads applied and the forces (or tractions) distributed over the elements discretizing the volume of the foundation is expressed by the following equation:

$$\{P\} = [R]^T \{t\} \tag{10}$$

On combining Equations (7), (8) and (10), we obtain the following equation:

$$\{P\} = \left([R]^T [G]^{-1} [R]\right)\{\Delta\} = \left[K(\omega)\right]\{\Delta\} \tag{11}$$

with ω denoting the circular frequency of vibration and $\left[K(\omega)\right]$ the impedance or dynamic-stiffness matrix of the rigid foundation.

Considering the incident plane SH, P, SV and R harmonic waves to be characterized by the vertical and horizontal angles of incidence, θ_V and θ_H, respectively, as shown in Figure 1, the motion of the half-space due to these seismic waves is expressed by the following equation:

$$\{u^f\} = \{U^f\} e^{\frac{-i\omega}{c}(x\cos\theta_H + y\sin\theta_H)} \tag{12}$$

Here, $\{U^f\} = \{U_x^f \quad U_y^f \quad U_z^f\}^T$ is known as the vector of amplitudes of the soil, which depends on the z coordinate if we want to study the case of embedded foundations. However, in the case of surface foundations (i.e., $z = 0$), this is known as the vector of the amplitudes of free-field displacements. Further, c denotes the apparent velocity of the incident waves, having the form $c = c_1/\cos\theta_V$ or $c = c_2/\cos\theta_V$ for P- or S-waves, respectively, and being equal to that for the R-wave. The explicit expressions of the vector $\{U^f\}$ for the SH-, P-, SV- and R-waves are given in Wong and Luco (1978).

The presence of a rigid foundation on the surface of the half-space results in the diffraction of the above waves so that the total displacement field $\{u\}$ is expressed by the equation,

$$\{u\} = \{u^f\} + \{u^s\} \tag{13}$$

where $\{u^s\}$ represents the scattered wave field in accordance with Equation (7). Also, the total displacement field in the contact region between the foundation and the half-space must be equal to the rigid-body motion of the foundation. On substituting Equation (8) into Equation (13), written in terms of the scattered field, the force-displacement relation is obtained as

$$\{u^s\} = [R]\{\Delta\} - \{u^f\} \tag{14}$$

This may be written in terms of the traction forces by describing the scattered wave field as in Equation (7), i.e.,

$$[G]\{t\} = [R]\{\Delta\} - \{u^f\} \tag{15}$$

which then leads to

$$\{t\} = [G]^{-1}[R]\{\Delta\} - [G]^{-1}\{u^f\} \tag{16}$$

On multiplying both sides of this equation by the transpose of the transformation matrix, we obtain

$$[R]^T\{t\} = [R]^T[G]^{-1}[R]\{\Delta\} - [R]^T[G]^{-1}\{u^f\} \tag{17}$$

Combining this with Equations (10) and (11) yields the external forces. The equilibrium between external forces and seismic forces can thus be described as follows:

$$\{P\} = [K]\{\Delta\} - [K^*]\{U^f\} \tag{18}$$

where

$$[K^*] = [R]^T[G]^{-1} e^{-i\omega(x\cos\theta_H + y\sin\theta_H)/c} \tag{19}$$

is the driving force matrix.

Equation (14) can be replaced by the alternative form,

$$\{\Delta\} = [C]\{P\} + [S^*]\{U^f\} \tag{20}$$

where $[C]$ (= $[K]^{-1}$) is the dynamic compliance matrix and $[S^*]$ is the input motion matrix given by the following expression:

$$[S^*] = [C][K^*] \tag{21}$$

When the rigid foundation is acted upon by the seismic waves only, the external forces are zero (i.e., $\{P\}$ = 0), and the seismic response of the foundation is obtained from Equation (18) or (20) by using the following expression:

$$\{\Delta\} = [S^*]\{U^f\} \tag{22}$$

with

$$[S^*] = \begin{bmatrix} S_{xx} & 0 & 0 \\ 0 & S_{yy} & S_{yz} \\ 0 & S_{zy} & S_{zz} \\ 0 & R_{xy} & S_{xz} \\ R_{yx} & 0 & 0 \\ S_{zx} & 0 & 0 \end{bmatrix} \tag{23}$$

When the mass of the foundation is not zero, one simply has to replace $[K]$ by $[K] - \omega^2[M]$ in the above equations, where $[M]$ is the mass matrix of the foundation.

VALIDATION OF THE METHOD

The accuracy of the BEM-TLM method used to study the three-dimensional response of foundations subjected to plane-harmonic waves with variable angles of incidence and frequencies of vibration is validated in this section through comparisons with the results obtained by Luco and Wong (1977) and Qian and Beskos (1996) for a semi-infinite ground. A parametric study is conducted to define the parameters of the calculation model. The influence of the discretization of the soil-foundation interface is studied. The thickness of a sublayer is taken small enough for the discrete model to transmit waves in an appropriate manner and without numerical distortions. This depends on the frequencies involved and the velocity of wave propagation. The frequency of loading and velocity of wave propagation affect the precision of the numerical solution. Kausel and Peek (1982) showed that the thickness of sublayer must be smaller than a quarter of the wavelength λ. Consequently, the maximum dimensionless frequency must not exceed N/4, where N represents the number of sublayers.

Consider a rigid, massless, square foundation of the side $B_x = 2a$ on the surface of the half-space with a Poisson's ratio ν = 1/3, such that it is subjected to the plane P, SV and SH harmonic waves with $\theta_H = 90^o$ and $\theta_V = 45^o$. Figure 4 shows the variations of the real and imaginary parts of the coefficient S_{xx} of movement with the dimensionless frequency $a_0 = \omega B/2C_s$. It is seen that the results obtained by the proposed method are in agreement with those obtained by Qian and Beskos (1996). On considering the same foundation when it is subjected to a horizontally incident Rayleigh wave (i.e., $\theta_H = 0^o$) and the corresponding velocity is taken as $c_R = 0.9325c$ for the Poisson's ratio ν = 1/3, Figure 5 shows the real and imaginary parts of the dimensionless displacement Δ_x/R_H as functions of the frequency a_0. These results based on the BEM-TLM method are seen to be in agreement with those of Qian and Beskos (1996) and Luco and Wong (1977) based on the BEM method, except for the differences for the dimensionless frequency a_0 higher than 2.5. These differences can be explained in following two ways:

1. Qian and Beskos (1996) have used isoparametric elements to determine the soil-foundation interface. These types of elements are more accurate than the constant elements used by the method proposed in this paper.
2. Qian and Beskos (1996) and Luco and Wong (1977) have used Green's functions of a semi-infinite soil, whereas the proposed method is based on Green's functions of a soil bounded by bedrock.

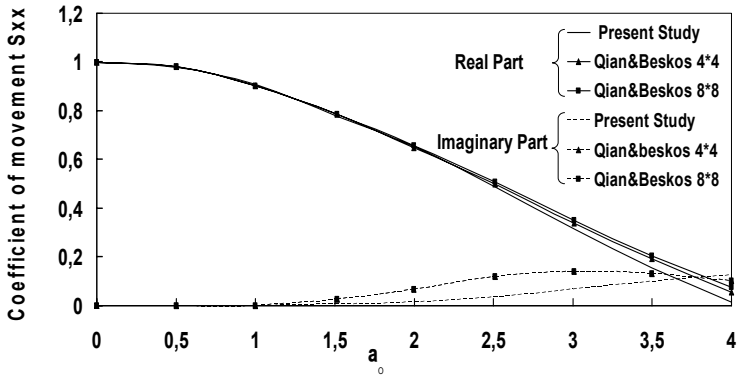

Fig. 4 Variation of coefficient S_{xx} of movement with dimensionless frequency a_0 for square foundation, $\theta_H = 0°$, $\theta_V = 45°$ and $c_s/c = 0.70711$

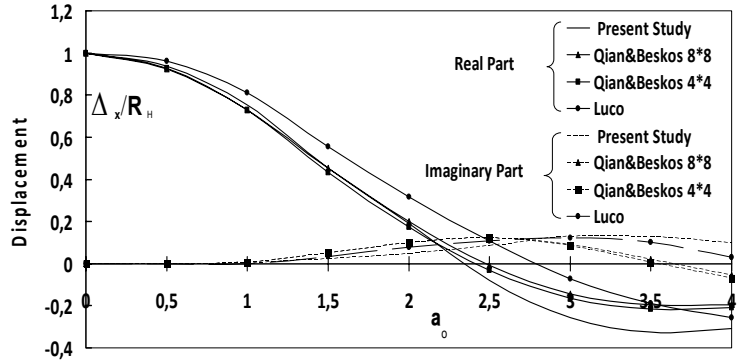

Fig. 5 Displacement response of square foundation under Rayleigh wave for $c_R/c = 0.9325$

PARAMETRIC STUDY AND DISCUSSION

1. Surface Foundation

In this section, a parametric analysis is performed for a square foundation of the side $B_x = 2a$ and subjected to the plane-harmonic waves with variable angles of incidence and frequencies of vibration (see Figure 1). The results are presented in terms of the coefficients of motion as functions of the

dimensionless frequency $a_0 = \omega B/2C_s$. The soil is characterized by the height $H_t = 10$ m of the bedrock (to simulate a semi-infinite soil medium), Poisson's ratio ν = 1/3, coefficient of hysteretic damping β = 0.05, shear modulus μ = 1 and density ρ = 1 g/cm^3. The terms of the coefficient of motion are presented in the figures below for the case of S-wave with the horizontal angle of incidence $\theta_H = 90^o$ and the vertical angle of incidence θ_V = 0^o, 30^o, 45^o, 60^o and 90^o.

1.1 Coefficients of Movements in Translation

For an angle of incidence θ_V = 90^o, the coefficients of translational movement, S_{xx}, S_{yy}, S_{zz}, are equal to unity for all the frequencies. Typically, this value is adopted in the study of a structure subjected to the seismic loading. This value induces oversized foundations. Figures 6 and 7 show that for other angles these coefficients vary with the dimensionless frequency. The amplitude of response also depends on the vertical angle of incidence. Further, it is seen that the real parts of S_{xx} and S_{zz} have higher magnitudes than the values of the imaginary parts. At low frequencies, the response is found to be in phase with the free-field motion. These coefficients filter low frequencies and therefore behave as low-pass filters.

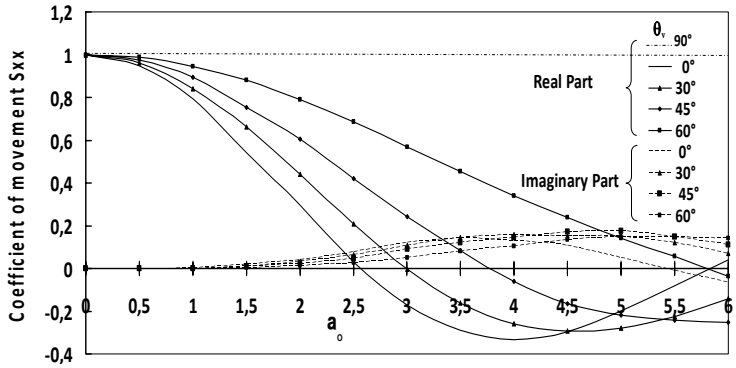

Fig. 6 Variation of coefficient S_{xx} of movement with dimensionless frequency a_0 for $\theta_H = 90°$

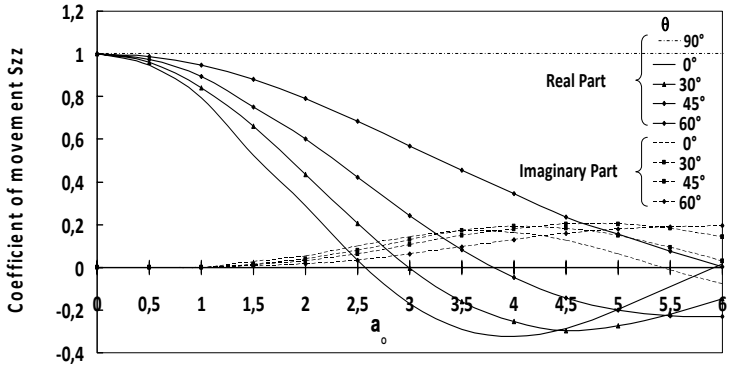

Fig. 7 Variation of coefficient S_{zz} of movement with dimensionless frequency a_0 for $\theta_H = 90°$

1.2 Coefficients of Movements in Rotation and Torsion

Figures 8 and 9 present the relative coefficients of the rotational movements, R_{xy} and R_{yx}, about the x-axis and y-axis, respectively. These coefficients are zero for an angle of incidence θ_V = 90^o and maximum for θ_V = 0^o. Figure 10 shows the relative coefficient of torsion, S_{zx}, about the *z*-axis as a function of dimensionless frequency for the vertical angle of incidence θ_V = 0^o, 30^o, 45^o and 60^o. These results show that the value of the imaginary part of S_{zx} is dominant. Thus, there is a large damping in the system. Also, the response is out of phase with the free-field motion at the center of the foundation. Figures 8–10 also show that these coefficients vary with the the vertical angle of incidence θ_V,

depending on the dimensionless frequency. Further, the amplitude of response depends on the vertical angle of incidence. The coefficients of movements of rotation and torsion filter high frequencies and therefore behave as high-pass filters.

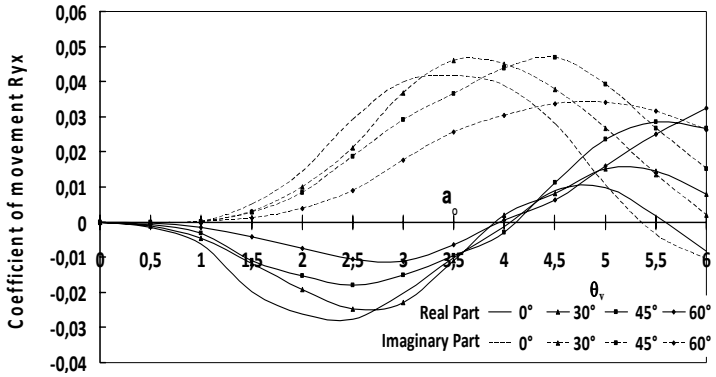

Fig. 8 Variation of coefficient R_{yx} of movement with dimensionless frequency a_0 for $\theta_H = 90°$

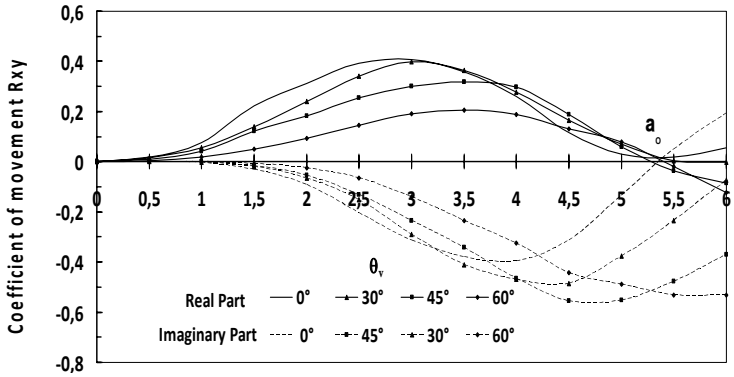

Fig. 9 Variation of coefficient R_{xy} of movement with dimensionless frequency a_0 for $\theta_H = 90°$

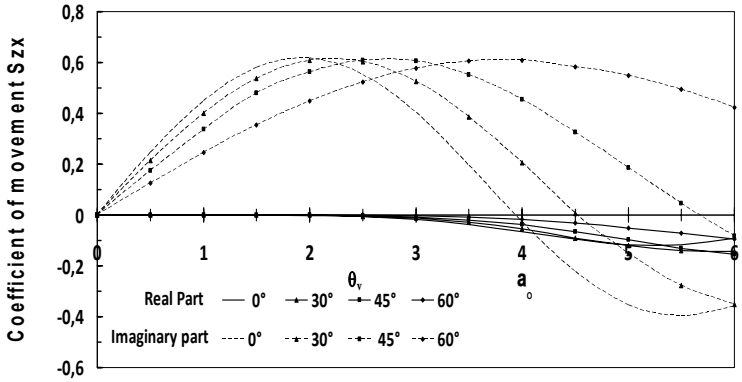

Fig. 10 Variation of coefficient S_{zx} of movement with dimensionless frequency a_0 for $\theta_H = 90°$

It may be mentioned that the matrix coefficients of movement shown in Figures 7–10 are valid only for $\theta_H = 90^o$, i.e., for S-waves with a horizontal angle of incidence. These coefficients can also be determined for other incidence angles and for other types of waves.

2. Embedded Foundation

In order to present results that are easier to understand visually, the driving-force vectors are converted to input-motion vectors by multiplying those with the inverse of the impedance matrix. Three different sets of results are given. The response of the massless foundation to the incident SH-, P- and

SV-type body waves is considered. Further, a square base of $B_x = 2a$ dimension, embedded in a homogeneous viscoelastic soil to the depth d, and subjected to the P-, SV- and SH-waves is considered (see Figure 11). The influence of the embedment ratio t ($= d/a$, taken as equal to 0, 0.3 and 0.6) on the seismic response of the foundation is studied. The results are presented in terms of displacements, rotations and torsion; these terms are calculated by using Equation (18) as the functions of the dimensionless frequency a_0. In order to simplify the presentation in this paper, only one direction of wave propagation is considered with the vertical incident angle θ_V taken as 45°. Figures 12–19 represent the terms of displacement, rotation and torsion caused by the incident P-, SV- and SH-waves. These curves are given for different values of relative embedment.

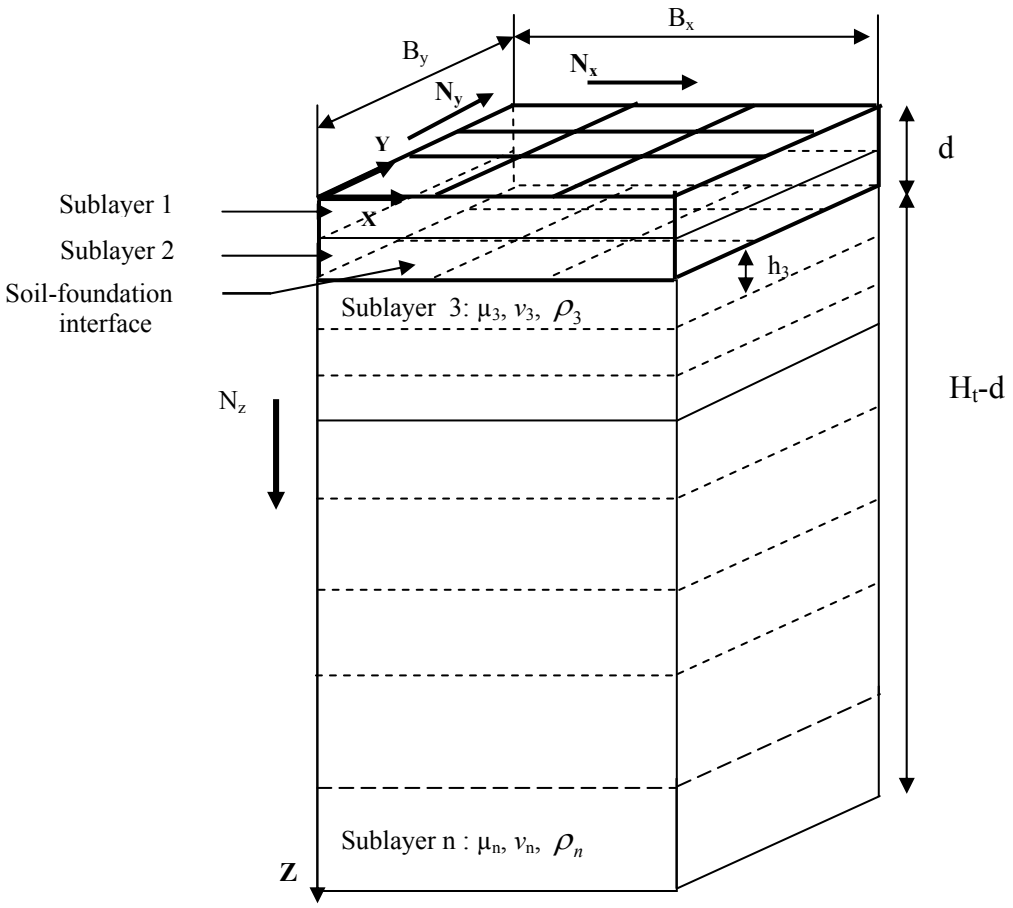

Fig. 11 Model of calculation for an embedded foundation subjected to harmonic seismic waves

2.1 Compression or P-Wave

The response of a massless foundation to an incident P-wave is considered. The wave travels in the x-direction with the particle motion taking place in the z- and x-directions. Except for the vertical incidence, i.e., θ_V = 90°, the incident P-wave causes a mode conversion, thus resulting in a reflected SV-wave. One angle of incidence is considered, which is equal to 45° (with respect to the x-axis). The wavelength of the incident P-wave is twice as long as that of the incident S-waves; therefore, the kinematic interaction now is less prominent. In general, the P-wave induces displacements along the x- and z-axes and rotation around the y-axis. Figures 12–14 respectively show the variations of displacements and rotation as the functions of dimensionless frequency, with the embedment coefficient t taken as 0, 0.3 and 0.6.

It may be observed that the displacements Δ_x and Δ_z and the rotation ϕ_y are strongly attenuated due to an increase in the embedment. Further, the horizontal displacement Δ_x is affected more by the

embedment than the vertical displacement Δ_z and rotation ϕ_y. It is seen that on increasing the embedment, the displacements and rotation are cancelled as the frequency decreases and then the signs change. The imaginary parts of the vertical and horizontal modes of translation are not affected by an increase in the embedment. In contrast, the imaginary part of the rotation is strongly affected by the embedment.

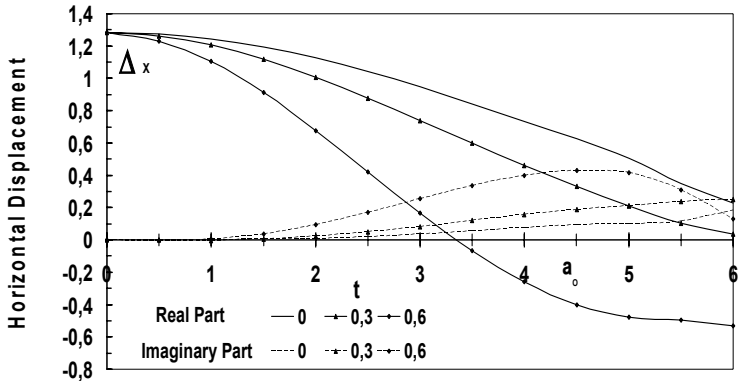

Fig. 12 Variations of horizontal input motion Δ_x due to incident P-wave with a_0 for $\theta_V = 45°$ and $\theta_H = 0°$

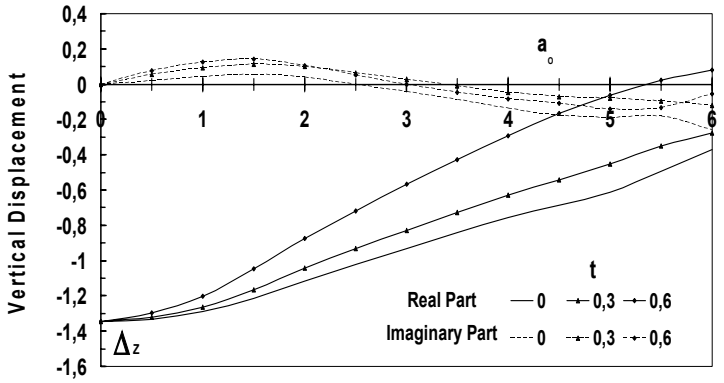

Fig. 13 Variations of horizontal input motion Δ_z due to incident P-wave with a_0 for $\theta_V = 45°$ and $\theta_H = 0°$

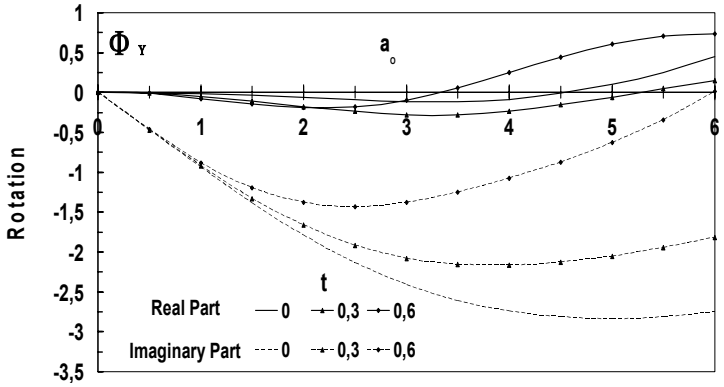

Fig. 14 Variations of rocking input motion ϕ_y due to incident P-wave with a_0 for $\theta_V = 45°$ and $\theta_H = 0°$

2.2 SV-Wave

The response of a massless foundation subjected to an incident SV-wave is considered. The wave travels in the x-direction with its particle motion in the z- and x-directions. For the vertical incident angle θ_V taken as 45°, the free-field motion for the SV-wave in the direction of propagation is zero. Further, similar to the case of P-wave, only the horizontal, vertical, and rocking components are excited. Figures 15–17 show the variations of displacements and rotation as the functions of frequency and thus show the influence of embedment on the motion of the foundation. Figure 15 shows that the displacement Δ_x is zero for a foundation on the surface (with t = 0). This, however, becomes non-zero for the relative embedment of t = 0.3 and 0.6, with the imaginary part getting strongly affected, and thus the foundation does not follow the free-field motion. Moreover, the horizontal displacement Δ_x is more affected by the presence of embedment than the vertical displacement Δ_z and the rotation ϕ_y, especially at low frequencies. The presence of embedment in the foundation just changes the signs of vertical displacement and rotation for the frequency a_0 greater than 4.

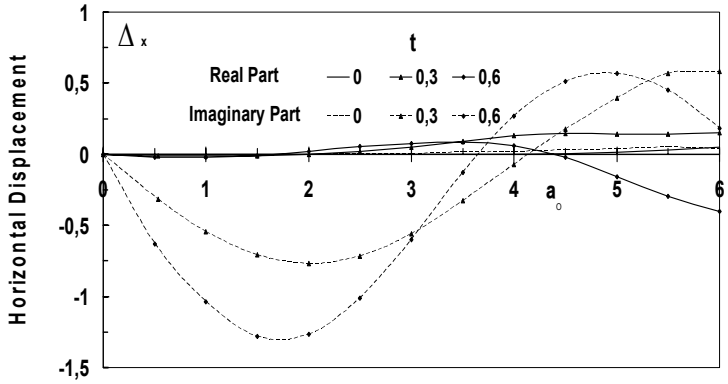

Fig. 15 Variations of horizontal input motion Δ_x due to incident SV-wave with a_0 for $\theta_V = 45°$ and $\theta_H = 0°$

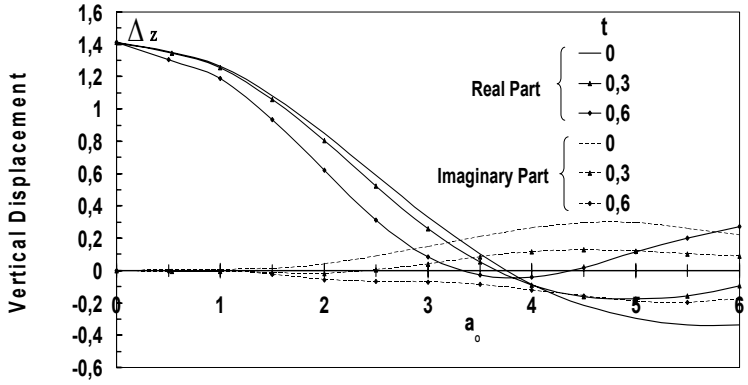

Fig. 16 Variations of vertical input motion Δ_z due to incident SV-wave with a_0 for $\theta_V = 45°$ and $\theta_H = 0°$

2.3 SH-Wave

The response of a square, massless foundation to a SH-wave is considered, with the horizontal angle of incidence θ_H taken as 90°. The incident wave travels in the y-direction; therefore, the particle motion of the wave is in the x-direction. This wave causes displacement and torsion in the foundation as shown in Figures 18 and 19 respectively for various cases of embedment (i.e., t = 0, 0.3 and 0.6). Figures 18 and 19 show that the horizontal displacement Δ_x and torsion ϕ_z are strongly affected by the embedment of

the foundation. For dimensionless frequencies lower than 3, Δ_x is not affected by increasing the relative embedment. This is however not the case for ϕ_z, which is strongly affected by an increase in the embedment. In contrast, for frequencies greater than 3, the presence of the foundation embedment causes a change in the signs of Δ_x and ϕ_z.

It is seen in all the above results for foundation embedment (see Figures 12–19) that the horizontal displacement caused by a P-wave is more attenuated than the displacement caused by a SH or SV-wave. On the other hand, the rotation caused by a SV-wave is more attenuated than the rotation caused by a P-wave.

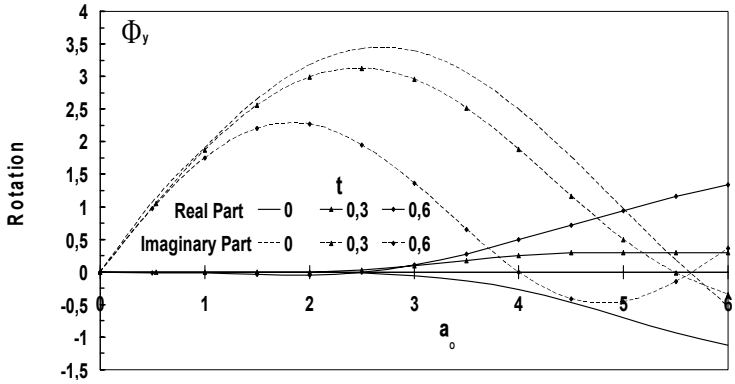

Fig. 17 Variations of rocking input motion ϕ_y due to incident SV-wave with a_0 for $\theta_V = 45°$ and $\theta_H = 0°$

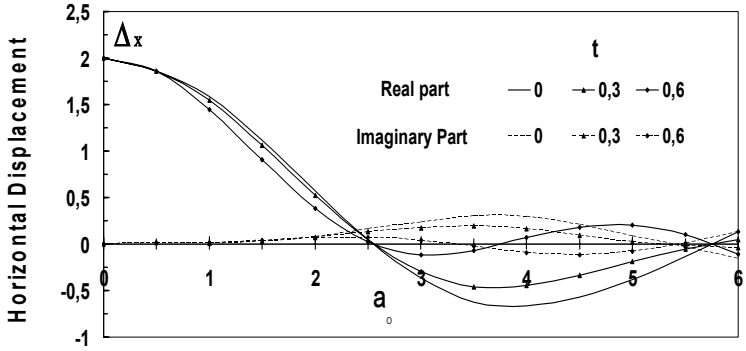

Fig. 18 Variations of horizontal input motion Δ_x due to incident SH-wave with a_0 for $\theta_V = 45°$ and $\theta_H = 90°$

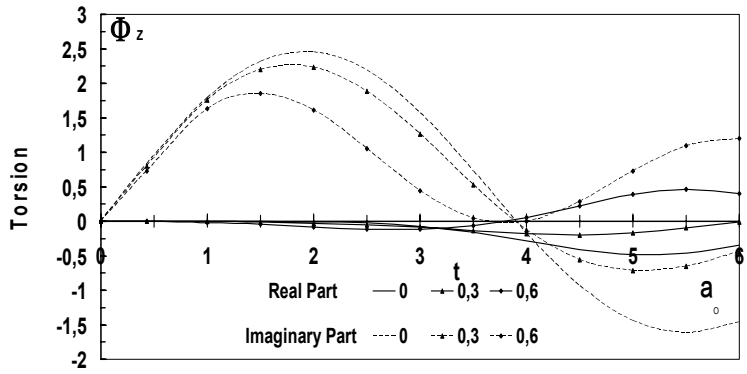

Fig. 19 Variations of torsion input motion ϕ_z due to incident SH-wave with a_0 for $\theta_V = 45°$ and $\theta_H = 90°$

CONCLUSIONS

The seismic response of a square, rigid foundation embedded in a homogeneous, viscoelastic soil and subjected to obliquely incident harmonic P-, SV-, SH- and R-waves has been formulated. A simplified BEM-TLM method has been developed and used to calculate the foundation-input motion under different travelling seismic waves. The solution has been formulated by using the boundary-element method in frequency domain while using the formalism of Green's functions. Constant quadrilateral elements have been used to obtain the seismic response based on this formulation. The efficiency of this method has been confirmed by comparison with the results of previous studies. This method is remarkably simple and has been concluded to be highly effective and economical to determine input motions for the rigid foundations of arbitrary geometry. The originality of the method lies first in the insignificance of the number of elements used in the discretization of the model and second in its ability to simulate a limited height of bedrock.

This study has also highlighted the importance of the inclination of incident waves on the behavior of a foundation. The results indicate the following:

- The response of a foundation subject to non-vertical incident waves is different from that of a foundation subject to vertically incident waves.
- Non-vertical incident waves generate torsion, translation, and rotation in the foundation, while vertically incident waves cause translation only.
- Assuming vertical angle of incidence (i.e., $\theta_V = 0^o$) leads to an oversizing of the foundations.
- The coefficients of translational movement filter low frequencies, while the coefficients of rotational movement filter high frequencies.
- The embedment of foundation affects displacement, rotation, and torsion in more specific ways and acts as a favorable factor in the seismic response of foundations. The movement of the foundation is strongly attenuated for foundations with relatively larger embedment depths, especially at low frequencies.

REFERENCES

1. Apsel, R.J. and Luco, J.E. (1987). "Impedance Functions for Foundations Embedded in a Layered Medium: An Integral Equation Approach", Earthquake Engineering & Structural Dynamics, Vol. 15, No. 2, pp. 213–231.
2. Aubry, D. and Clouteau, D. (1992). "A Subdomain Approach to Dynamic Soil-Structure Interaction" in "Recent Advances in Earthquake Engineering and Structural Dynamics (edited by V.E. Davidovici)", Ouest Éditions, Presses Académiques, Nantes, France.
3. Beskos, D.E. (1987). "Boundary Element Methods in Dynamic Analysis", Applied Mechanics Reviews, Vol. 40, No. 1, pp. 1–23.
4. Boumekik, A. (1985). "Fonctions Impédances d'une Fondation Vibrante en Surface ou Partiellement Encastrée dans un sol Multicouche", Ph.D. Thesis, Université Libre de Bruxelles, Brussels, Belgium (in French).
5. Çelebi, E., Fırat, S. and Çankaya, İ. (2006). "The Evaluation of Impedance Functions in the Analysis of Foundations Vibrations Using Boundary Element Method", Applied Mathematics and Computation, Vol. 173, No. 1, pp. 636–667.
6. Fujimori, T., Tsunoda, T., Izumi, M. and Akino, K. (1992). "Partial Embedment Effects on Soil-Structure Interaction", Proceedings of the Tenth World Conference on Earthquake Engineering, Madrid, Spain, Vol. 3, pp. 1713–1718.
7. Imamura, A., Watanabe, T., Ishizaki, M. and Motosaka, M. (1992). "Seismic Response Characteristics of Embedded Structures Considering Cross Interaction", Proceedings of the Tenth World Conference on Earthquake Engineering, Madrid, Spain, Vol. 3, 1719–1724.
8. Karabalis, D.L. and Mohammadi, M. (1998). "3-D Dynamic Foundation-Soil-Foundation Interaction on Layered Soil", Soil Dynamics and Earthquake Engineering, Vol. 17, No. 3, pp. 139–152.
9. Kausel, E. and Peek, R. (1982). "Dynamic Loads in the Interior of a Layered Stratum: An Explicit Solution", Bulletin of the Seismological Society of America, Vol. 72, No. 5, pp. 1459–1481.

10. Kausel, E. and Roësset, J.M. (1981). "Stiffness Matrices for Layered Soils", Bulletin of the Seismological Society of America, Vol. 71, No. 6, pp. 1743–1761.
11. Kausel, E., Whitman, R.V., Morray, J.P. and Elsabee, F. (1978). "The Spring Method for Embedded Foundations", Nuclear Engineering and Design, Vol. 48, No. 2-3, pp. 377–392.
12. Lin, H.-T. and Tassoulas, J.L. (1986). "A Hybrid Method for Three-Dimensional Problems of Dynamics of Foundations", Earthquake Engineering & Structural Dynamics, Vol. 14, No. 1, pp. 61–74.
13. Liou, G.-S. (1993). "Impedance for Rigid Square Foundation on Layered Medium", Structural Engineering/Earthquake Engineering, JSCE, Vol. 10, No. 2, pp. 83s–93s.
14. Liou, G.-S. and Chung, I.L. (2009). "Impedance Matrices for Circular Foundation Embedded in Layered Medium", Soil Dynamics and Earthquake Engineering, Vol. 29, No. 4, pp. 677–692.
15. Luco, J.E. and Wong, H.L. (1977). "Dynamic Response of Rectangular Foundations for Rayleigh Wave Excitation", Proceedings of the Sixth World Conference on Earthquake Engineering, New Delhi, Vol. II, pp. 1542–1547.
16. Lysmer, J. and Waas, G. (1972). "Shear Waves in Plane Infinite Structures", Journal of the Engineering Mechanics Division, Proceedings of ASCE, Vol. 98, No. EM1, pp. 85–105.
17. McKay, K. (2009). "Three Applications of the Reciprocal Theorem in Soil-Structure Interaction", Ph.D. Dissertation, University of Southern California, Los Angeles, U.S.A.
18. Mizuhata, K., Kusakabe, K. and Shirase, Y. (1988). "Study on Dynamic Characteristics of Embedded Mass and Its Surrounding Ground", Proceedings of Ninth World Conference on Earthquake Engineering, Tokyo-Kyoto, Japan, Vol. III, pp. 679–684.
19. Mohammadi, M. (1992). "3-D Dynamic Foundation-Soil-Foundation Interaction by BEM", Ph.D. Dissertation, Department of Civil Engineering, University of South Carolina, Columbia, U.S.A.
20. Ohtsuka, Y., Fukuoka, A., Akino, K. and Ishida, K. (1996). "Experimental Studies on Embedment Effects on Dynamic Soil-Structure Interaction", Proceedings of the Eleventh World Conference on Earthquake Engineering, Acapulco, Mexico, Paper No. 59 (on CD).
21. Pecker, A. (1984). "Dynamique des Sols", Presses de l'Ecole Nationale des Ponts et Chaussées, Paris, France (in French).
22. Qian, J. and Beskos, D.E. (1996). "Harmonic Wave Response of Two 3-D Rigid Surface Foundations", Soil Dynamics and Earthquake Engineering, Vol. 15, No. 2, pp. 95–110.
23. Sbartai, B. and Boumekik, A. (2006). "Vertical Compliance Function of Adjacent Surface Rigid Footings in Heterogeneous Soil Layer", Proceedings of the Sixth European Conference on Numerical Methods in Geotechnical Engineering, Graz, Austria, pp. 217–222.
24. Sbartai, B. and Boumekik, A. (2007). "Horizontal Compliance Function of Adjacent Surface Rigid Footings in Homogeneous Soil Limited by a Substratum", Proceedings of the Fourth International Conference on Earthquake Geotechnical Engineering, Thessaloniki, Greece, Paper No. 1729 (on CD).
25. Sbartai, B. and Boumekik, A. (2008). "Ground Vibration from Rigid Foundation by BEM-TLM", ISET Journal of Earthquake Technology, Vol. 45, No. 3-4, pp. 65–78.
26. Spyrakos, C.C. and Xu, C. (2004). "Dynamic Analysis of Flexible Massive Strip-Foundations Embedded in Layered Soils by Hybrid BEM-FEM", Computers & Structures, Vol. 82, No. 29-30, pp. 2541–2550.
27. Suárez, M., Avilés, J. and Sánchez-Sesma, F.J. (2002). "Response of L-Shaped Rigid Foundations Embedded in a Uniform Half-Space to Traveling Seismic Waves", Soil Dynamics and Earthquake Engineering, Vol. 22, No. 8, pp. 625–637.
28. Watakabe, M., Matsumoto, H., Ariizumi, K., Fukahori, Y., Shikama, Y., Yamanouchi, K. and Kuniyoshi, H. (1992). "Earthquake Observation of Deeply Embedded Building Structure", Proceedings of the Tenth World Conference on Earthquake Engineering, Madrid, Spain, Vol. 3, pp. 1831–1838.
29. Wong, H.L. and Luco, J.E. (1978). "Dynamic Response of Rectangular Foundations to Obliquely Incident Seismic Waves", Earthquake Engineering & Structural Dynamics, Vol. 6, No. 1, pp. 3–16.
30. Wong, H.L. and Luco, J.E. (1986). "Dynamic Interaction between Rigid Foundations in a Layered Half-Space", Soil Dynamics and Earthquake Engineering, Vol. 5, No. 3, pp. 149–158.

INSTRUCTIONS TO AUTHORS

1. Research papers, technical notes, state-of-the-art papers and reports on damaging earthquakes which have not been previously published or offered for publication elsewhere are considered for publication in the ISET Journal of Earthquake Technology. Discussions on any paper previously published in the Journal are also considered for publication. Articles submitted to the Journal should be original and should not be under consideration for publication elsewhere at the same time.

2. The PDF file of the manuscript should be submitted to the Editor electronically at ***vinaykg@iitk.ac.in*** for possible publication of an article in the Journal. The submission may alternatively be made to an Associate Editor: at ***manohar@civil.iisc.ernet.in*** for papers related to *Structural Dynamics*; at ***ramana@civil.iitd.ernet.in*** for *Soil Dynamics,* and ***mukutfeq@iitr.ernet.in*** for *Seismology and Seismotectonics*.

3. Following are specific requirements with regard to articles and formats:

   i. Paper length: The length of a paper should be restricted to 10000 words maximum

   ii. Headings and subheadings: Headings should be in bold uppercase and not numbered. Sub-headings should be in bold lower case and may be numbered.

   iii. Figures and Tables: These should be numbered consecutively in Arabic numerals and should be titled. Figure captions should be given on a separate sheet.

   iv. Photographs, illustrations: Good glossy bromide prints of these must accompany the manuscript and not be attached to the manuscript pages.

   v. References: These should be listed alphabetically at the end of the text and numbered serially. These should be cited in the text by the last name(s) of authors followed by the year of publication in parenthesis. In case of more than two authors, the last name of the first author followed by et al. and the year of publication is to be cited in the text. References are to be listed in the following format only:

      1. Krishna, J. and Chandrasekaran, A.R. (1964). "Earthquake Resistant Design of an Elevated Water Tower", Bull. Indian Soc. of Earthquake Tech., Vol. 1, No. 1, pp. 20-36.
      2. Prakash, S. (1960). "Soil Dynamics", McGraw Hill Book Co., New Delhi.
      3. Wason, H.R., Sharma, M.L., Pal, K. and Srivastava, L.S. (1986). "Digital Telemetered Seismic Array in Ganga-Yamuna Valley", Proc. 8th Symposium on Earthquake Engg., Roorkee, Vol. 2, pp. 91-99.
      4. Rai, D.C., Narayan, J.P., Pankaj and Kumar, A. (1997). "Jabalpur Earthquake of May 22, 1997: Reconnaissance Report", Deptt. of Earthquake Engineering, University of Roorkee, Roorkee.

   vi. Abstract: This should not exceed 150 words and be an abbreviated, accurate representation of the contents of the article. It should be followed by a list of 3 to 5 key words of these contents.

   vii. Units: All quantities should be in SI units. Other units may be enclosed in parentheses after the SI units, if necessary.

4. **Preparation for Publication:** Once accepted for publication, the final version of the article will be sent to the author(s) for proof checking. The author(s) should ensure that it is complete with no grammatical or spelling errors and return the same to the Co-Editor within 15 days.

ISSN 0972-0405

ISET JOURNAL OF EARTHQUAKE TECHNOLOGY

Vol. 49 No. 1-2 March-June 2012

CONTENTS

No.	Paper	Page
518	Seismic Retrofit of Beams in Buildings for Flexure Using Concrete Jacket **V.T. Badari Narayanan, Amlan Kumar Sengupta and S.R. Satish Kumar**	1
519	NN-Based Damage Detection in Multi-storey Buildings from Modal Parameter Changes **Hemant Kumar Vinayak, Ashok Kumar, Pankaj Agarwal and Shashi Kant Thakkar**	23
520	Effect of Seismic Oblique Waves on Dynamic Response of an Embedded Foundation **Salah Messioud, Badreddine Sbartai and Daniel Dias**	37

Financial Assistance from DST, New Delhi for the Publication of ISET Journals for 2011–2012 and 2012–2013 is duly acknowledged

Published by : Dr. Ajay Chourasia, Co-Editor (2011-2013), Indian Society of Earthquake Technology, Roorkee
Printed at : R.K. Printers, RKE # Ph. : 01332-270957, 9897276995 E-mail : rkprint270957@gmail.com